공학박사학위논문

Extension of biotic ligand model to the prediction of site-specific ecological risk of arsenate in *Aliivibrio fischeri* and *Hordeum vulgare*

Aliivibrio fischeri 및 *Hordeum vulgare* 에 대한
비소의 현장특이적 생태위해성 예측을 위한
biotic ligand model 의 확장

2018 년 8 월

서울대학교 대학원
건설환경공학부
안진성

Extension of biotic ligand model to the prediction of site-specific ecological risk of arsenate in *Aliivibrio fischeri* and *Hordeum vulgare*

by

Jinsung An

Advisor: Kyoungphile Nam

A dissertation submitted in partial fulfillment

of the requirements for the degree of

Doctor of Philosophy

Department of Civil and Environmental Engineering

The Graduate School

SEOUL NATIONAL UNIVERSITY

August 2018

Abstract

Extension of biotic ligand model to the prediction of site-specific ecological risk of arsenate in *Aliivibrio fischeri* and *Hordeum vulgare*

Jinsung An
Department of Civil and Environmental Engineering
The Graduate School
Seoul National University

The effectiveness of *in situ* stabilization in arsenic (As)-contaminated soil, as one of risk mitigation measures, should be evaluated by means of both chemical extractability and biological responses, as chemical analysis alone may not be sufficient to assess the ecotoxicity. Although bioassays are liable and realistic in determining As toxicity in soil, they are time-consuming and costly. As an alternative, a biotic ligand model (BLM) was developed to predict the site-specific toxicity of inorganic arsenate (iAs(V)) in soil porewater by using the bioluminescent bacteria

Aliivibrio fischeri. To enhance the accuracy of the BLM, the effects of major cations/anions; pH; and humic acid (HA), used as a surrogate of dissolved organic matter, were assessed, and incorporated into the BLM.

As the pH increased from 5 to 9, the $HAsO_4^{2-}$ form was more predominant than $H_2AsO_4^-$, and the $EC_{50}[As]_T$ (50% effective iAs(V) concentration) decreased drastically from 3554 ± 393 to 39 ± 6 μM; thus, the $HAsO_4^{2-}$ form was more toxic to *A. fischeri* than $H_2AsO_4^-$ was. As the HPO_4^{2-} activity increased from 0 to 0.44 mM, the $EC_{50}\{HAsO_4^{2-}\}$ values (50% effective $HAsO_4^{2-}$ activity) increased from 31 ± 6 to 859 ± 128 μM, indicating that the toxicity of iAs(V) decreased, owing to the competition caused by the structural similarity between iAs(V) and phosphate ions. However, the activities of Ca^{2+}, Mg^{2+}, K^+, SO_4^{2-}, NO_3^-, and HCO_3^- did not significantly affect the $EC_{50}\{HAsO_4^{2-}\}$ values. The BLM was reconstructed to account for the effects of pH and phosphate, and the conditional binding constants for $H_2PO_4^-$, HPO_4^{2-}, $H_2AsO_4^-$, and $HAsO_4^{2-}$ binding to the active binding sites of *A. fischeri* were obtained: 3.424 for $\log K_{XH2PO4}$, 4.588 for $\log K_{XHPO4}$, 3.067 for $\log K_{XH2AsO4}$, and 4.802 for $\log K_{XHAsO4}$. The fraction of active binding sites that need to be occupied by iAs(V) to induce 50% toxicity ($f_{mix}^{50\%}$) was found to be 0.616.

This type of approach can be extended to a higher plant (i.e., barley *Hordeum vulgare*) via an interspecies extrapolation approach. The extrapolated BLM, which only considers inherent sensitivity, could explain well the alteration of iAs(V) toxicity by the competition effect of phosphate. In addition, the fact that the $EC_{50}\{HAsO_4^{2-}\}$ decreased from 45.1 ± 4.34 to 15.0 ± 2.60 μM as Ca^{2+} concentration increased from 0.2 to 20 mM, owing to the accumulation of $H_2AsO_4^-$ and $HAsO_4^{2-}$

on the cell membrane surface, can be successfully considered in the extrapolated BLM by using a linear relationship between cell membrane surface electrical potential and $EC_{50}\{HAsO_4^{2-}\}$.

Finally, the feasibility of direct analysis of the binding resin in the DGT using X-ray fluorescence spectrometry (XRF) was investigated to simplify the analytical procedures used to determine bioavailable As concentrations in soil. The binding resin obtained from the DGT was dried at 25°C in a desiccator with silica gel for 2 h, and then directly analyzed via XRF. The As mass loaded in the DGT binding resin was plotted against the X-ray intensity obtained from the XRF analysis to generate a calibration curve, which showed good linearity (determination coefficient; R^2 = 0.997) with a detection limit of 0.06 μg. A correction factor (CF) for compensating the spectral interference of Pb was determined by considering the slope between the X-ray intensity measured at a *Bragg* angle of 48.781° for As-Kα and the Pb mass on the DGT binding resin. The use of the derived CF value (0.113) is reasonable for obtaining As concentrations with high accuracy.

The overall results of thesis demonstrate that the toxicity and/or bioavailability of iAs(V)-contaminated soil can be effectively predicted by using the extended BLM in conjunction with the chemical analysis data of the soil porewater.

Keywords: Inorganic arsenate, biotic ligand model, diffusive gradients in thin film, interspecies extrapolation, soil porewater

Student Number: 2014-31121

Table of Contents

List of Tables

List of Figures

CHAPTER 1

Introduction

1.1. General overview

Many lines of evidence demonstrate that total concentrations of metals and metalloids in soil are not commensurate with the available fractions to soil biota [1,2]. This phenomenon occurs mainly due to the complex interactions of metals and metalloids with components of soil and soil solution (e.g., organic carbon content, clay content, dissolved organic carbon concentration, pH, and cations/anions concentrations) which commonly results in altered bioavailability and toxicity. Hence, the determination of the site-specific bioavailability and toxicity of metals and metalloids-contaminated soil is crucial for realistic ecological risk characterization.

Significant portions of this chapter were published in An et al. ("Journal of Hazardous Materials, 203-204, Jinsung An, Seulki Jeong, Hee Sun Moon, Eun Hea Jho, Kyoungphile Nam, Prediction of Cd and Pb toxicity to *Vibrio fischeri* using biotic ligand-based models in soil, 69-76, Copyright Elsevier (2012)", "Microchemical Journal, 120, Jinsung An, Junseok Lee, Gyuri Lee, Kyoungphile Nam, Hye-On Yoon, Combined use of collision cell technique and methanol addition for the analysis of arsenic in a high-chloride-containing sample by ICP-MS, 77-81, Copyright Elsevier (2015)") with permission from Elsevier.

An appropriate assessment of toxicity of metals and metalloids in soil has been paid a great attention, and some readily available tools exist. Measure of toxicity of metals and metalloids in soil may be accomplished by direct biological means [3]. Biological methods (e.g., activity of microorganisms, bioaccumulation or toxicity tests of plants and soil invertebrates) are reliable and realistic in determining toxicity of metals and metalloids in soil, but they are time-consuming and costly.

As an alternative, biotic ligand model (BLM) was widely used to predict the metal toxicity in water body [4,5]. Recently, terrestrial biotic ligand model (TBLM) [6,7] modified from BLM has been proposed as a promising tool for assessing metal toxicity in soil. It is a semi-mathematical model to predict metal toxicity in soil by using soil porewater chemistry (i.e., dissolved metal concentration, pH, dissolved organic carbon, and concentrations of major cations/anions) [7,8]. TBLM supposes that metal ions adsorb to soil matrix and those present in soil solution exist as an equilibrium state, and free metal ions in soil solution bind to the active sites (i.e., biotic ligands; BL) of organisms, causing toxic effect. In addition, it is assumed that major cations (e.g., Ca^{2+}, Mg^{2+}, K^{+}) present in soil solution compete with free metal ions for the BL sites, and such competition mitigates the toxicity of free metal ions.

Arsenic (As) is a metalloid that is highly toxic to living organisms in the environment [9,10]. It is widely spread in the aquatic and terrestrial environments via both natural and anthropogenic sources. It is produced through a number of pathways such as agricultural usages (e.g., pesticides, herbicides, and fertilizers), wood preservatives (e.g., chromate copper arsenate), and industrial byproducts (e.g., smelter wastes and coal combustion ash) [11-13]. In addition, high As concentrations in groundwater, which naturally occur from As-bearing minerals (e.g., arsenopyrite

(FeAsS)), have been found in several countries and threaten human health and the integrity of ecosystems [9].

Despite the extensive previous studies for cationic metals, application of the BLM approach to predict As toxicity is very few, because inorganic arsenate (iAs(V)), that is a predominant form in various As species, is present as oxyanions (i.e., $H_2AsO_4^-$, $HAsO_4^{2-}$). In consequence, the BLM should be reconstructed to adequately predict iAs(V) toxicity, and its parameters should be determined, since understanding the iAs(V) toxicity in soil porewater is important in realistic ecological risk characterization.

1.2. Background

1.2.1. Mathematical description of BLM for cationic metals

Metals and cations present in solution react with BL sites (i.e., active binding sites located in negative charged cell membrane surface) of an organism. The overall process can be expressed with the conditional binding constant as follows.

$$K_{MBL} = \frac{[MBL^+]}{\{M^{2+}\}[BL^-]} \quad (1.1)$$

Where $[MBL^+]$ is the concentration of metal-*BL* complex (mol/L), $\{M^{2+}\}$ is the activity of free metal ion (mol/L), $[BL^-]$ is the concentration of unoccupied *BL* sites

(mol/L), and K_{MBL} is the conditional binding constant for metal bound to *BL* sites (L/mol). The BL sites can be occupied by competing cations (e.g., Ca^{2+}, Mg^{2+}, K^{+}), and the complexation reaction can be also expressed in Eq. 1.1. The concentration of the total BL sites ([*TBL*]) can be expressed as Eq. 1.2, and substituting Eq. 1.2 with Eq. 1.1 yields Eq. 1.3.

$$[TBL] = [BL^-] + [CaBL^+] + [MgBL^+] + [KBL] + [MBL^+] \tag{1.2}$$

$$[TBL] = [BL^-](1 + K_{CaBL}\{Ca^{2+}\} + K_{MgBL}\{Mg^{2+}\} + K_{KBL}\{K^+\} + K_{MBL}\{M^{2+}\}) \tag{1.3}$$

The fraction of *BL* sites occupied by metals (*f*) is proportional to the toxicity imposed on an organism followed by the main hypothesis of the BLM (Eq. 1.4) [14]. The EC_{50} values can be expressed as follows (Eq. 1.5).

$$f = \frac{[MBL^+]}{[TBL]} = \frac{K_{MBL}\{M^{2+}\}}{1 + K_{CaBL}\{Ca^{2+}\} + K_{MgBL}\{Mg^{2+}\} + K_{KBL}\{K^+\} + K_{MBL}\{M^{2+}\}} \tag{1.4}$$

$$EC_{50}\{M^{2+}\} = \frac{f_{MBL}^{50\%}(1 + K_{CaBL}\{Ca^{2+}\} + K_{MgBL}\{Mg^{2+}\} + K_{KBL}\{K^+\})}{(1 - f_{MBL}^{50\%})K_{MBL}} \tag{1.5}$$

Where $EC_{50}\{M^{2+}\}$ is the free metal ion activity resulting in 50% toxic effect and $f_{MBL}^{50\%}$ is the *BL* sites needed to be occupied by a free metal ion to cause 50% toxic effect.

Conditional binding constants of competing cations (i.e., K_{CaBL}, K_{MgBL}, K_{KBL}) were derived from the slopes and intercepts of the linear relationships using Eq. 1.5. The K_{MBL} and $f_{MBL}^{50\%}$ were determined by optimizing the linear relationship between the logit-transformed toxic effect and the fraction of *BL* sites occupied by metals while changing K_{MBL} values [14].

As presented above, the main assumption of the BLM for cationic metals is that positively charged free metal ions bind to the negatively charged BL sites on the cell membrane surface. To this regard, it was assumed that the active binding site (ABS) on the cell membrane, that is positively charged, can attach oxyanions in this study.

1.2.2. Soil porewater toxicity as an indicator of soil toxicity

There are two methods of bioassay for soil or sediment: the use of soil/sediment itself or its suspension, and the use of its elutriate [15]. The appropriate method and test species have to be selected based on the exposure route of contaminants to the target receptor. For example, in the case of absorbing nutrients through roots like plants, it is reasonable to use the method using elutriates. On the other hand, if there is a possibility for receptors to react with gut juice by ingesting soil/sediment like earthworms, it is reasonable to use the method using the soil/sediment itself or its suspension.

Anderson et al. [16] confirmed the similarity of the survival rate of *Rhepoxynius abronius* to sediments contaminated with dichlorodiphenyldichloroethylene at Terminal Island (CA, USA) and the embryo development rate of *Haliotis rufescens*

to the porewater recovered from the same sediments. In addition, Hunt et al. [17] reported the similarity of the survival rate of *Ayarnangra estuarius* to sediments contaminated with Ni and Cr at Paradise cove (CA, USA) and the embryo development rate of *Strongylocentrotus purpuratus* to the same sediments. Although different species were used depending on the type of contact medium, there are high correlations between sediment toxicity and porewater toxicity.

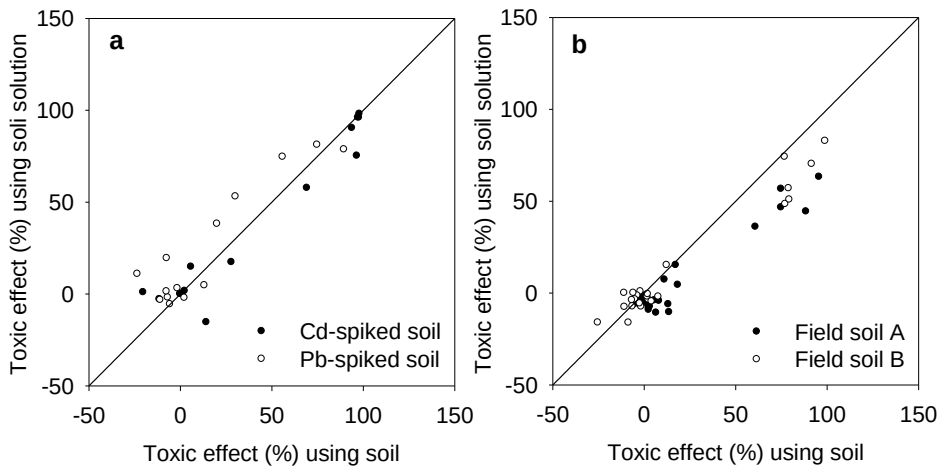

Figure 1.1. Comparison of experimentally determined toxic effects (i.e., % bioluminescence inhibition) between soil and soil solution after 5-min exposure; (a) pristine soils freshly spiked with Cd or Pb and (b) field-aged soils contaminated with various heavy metals (i.e., Cd, Pb, Cu, As). Open and closed circles on the solid line means that the toxicity in soil and soil solution is the same.

An et al. [18] observed that the strong linearity between soil suspension toxicity and soil solution toxicity. To test whether or not the use of soil solution instead of soil suspension was valid, Cd and Pb toxicity in soil solution was compared to their

toxicity in soil suspension [18]. The inhibition of bioluminescence was experimentally determined in soil and soil solution after 5-min exposure to *Aliiibrio fischeri*. For this experiment, pristine soil freshly spiked with Cd or Pb and field-aged soil contaminated with various metals (i.e., Cd, Pb, Cu, As) were used. The former was considered to have easily desorbable metals and the latter as a medium containing strongly sorbed metals. Toxicity data from both soil samples resulted in strong positive linear relationships of toxic effects (i.e., bioluminescence inhibition) between the soil and the soil solution with the correlation coefficients of above 0.9 ($p < 0.005$) (Figure 1.1). Student's *t*-test results (i.e., $p > 0.05$ in all cases) confirmed no significant difference in toxic effects between the soil and the soil solution. The results clearly demonstrate that metal toxicity to *A. fischeri* only originates from the dissolved metal ions and, if any, the metal ions associated with particles passed through the 0.45-μm GHP syringe filter. It indicates that soil solution toxicity can be reliably used to represent the toxicity in both freshly spiked and field-aged soils.

In the light of these facts, it is reasonable to predict soil toxicity by developing a toxicity prediction model (i.e., biotic ligand model) in conjunction with the chemical analysis data of the soil porewater (soil solution).

1.2.3. *In situ* stabilization as a risk mitigation measure for As-contaminated soil

Stabilization is a method to reduce mobility and bioavailability of contaminants by injecting a stabilizing agent into the environmental medium to change the contaminant into a chemically and biologically stable form [19,20]. According to USEPA [21], the stabilization/solidification method has been applied to about 25%

of the Superfund site. The stabilization method is to inject appropriate stabilizing agents into the soil depending on the type and site characteristics of the contaminant, and it can be effectively applied in areas where it is difficult to purify by active treatment which requires closure or excavation such as soil washing [22]. However, since this approach is a kind of risk mitigation measure, it does not reduce total contaminant concentration in soil, but blocks the exposure routes. Hence, the continuous monitoring including chemical extractability of contaminants and biological responses (ecotoxicity) of the site where the stabilization was employed is required. In this thesis, the chemical extractability and ecotoxicity of As-contaminated soil before and after employing stabilization technique were tested, and the importance of evaluating (or predicting) ecotoxicity was emphasized.

1.3. Research Objectives

The primary objective of this thesis was to develop BLM for predicting site-specific inorganic arsenate (iAs(V)) toxicity in soil porewater, because chemical extractability of iAs(V) in soil alone may not be sufficient to assess the ecotoxicity (chapter 2). To consider the effect of various environmental factors (i.e., pH, phosphate) that influence iAs(V) toxicity, the extended BLM was developed with derivation of its parameters (i.e., K_{XHAsO4}, $K_{XH2AsO4}$, K_{XHPO4}, K_{XH2PO4}, $f_{mix}^{50\%}$) (chapter 3). An interspecies extrapolation of the developed BLM from *A. fischeri* to a higher terrestrial plant barley *Hordeum vulgare* was conducted with consideration of cell

membrane surface electrical potential, which significantly affects iAs(V) toxicity to plants, not *A. fischeri* (chapter 4). To simply and rapidly determine bioavailable (labile) iAs(V) concentrations in soil, the combined use of DGT and X-ray fluorescence spectrometry was proposed (chapter 5).

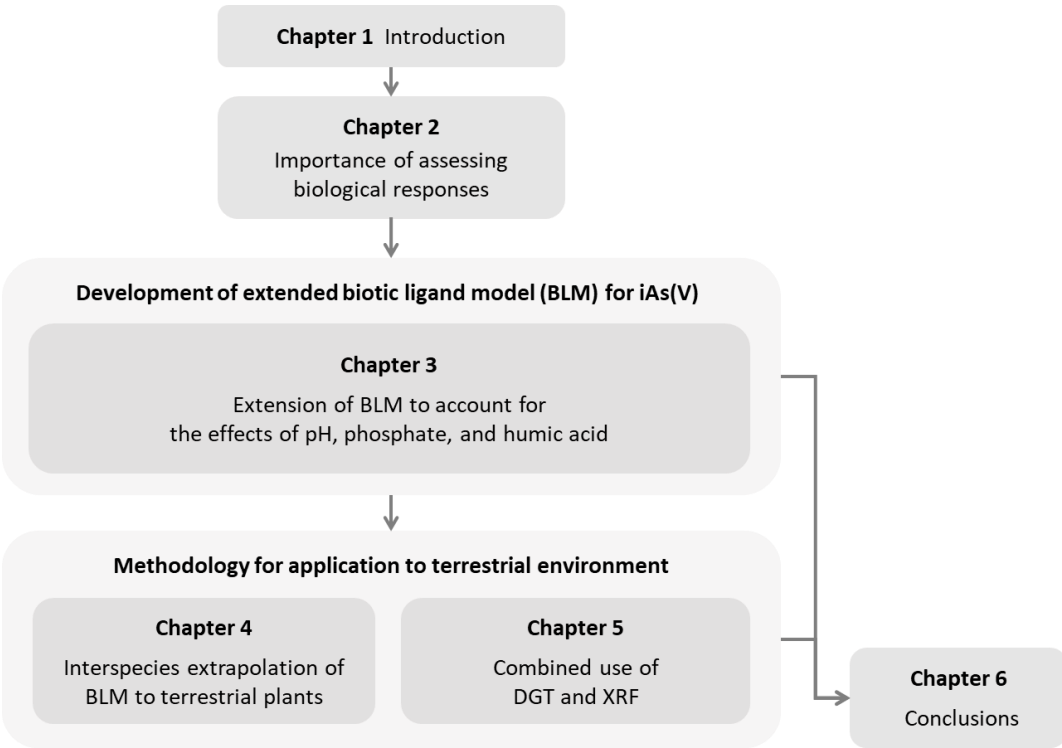

Figure 1.2. Dissertation structure

References

[1] W.J.G.M. Peijnenburg, T. Jager, Monitoring approaches to assess bioaccessibility and bioavailability of metals: matrix issues, Ecotoxicol. Environ. Saf. 56 (2003) 63-77.

[2] K. Lock, C.R. Janssen, Influence of aging on metal availability in soils, Rev. Environ. Contam. Toxicol. 178 (2003) 1-21.

[3] R. Lanno, J. Wells, J. Conder, K. Bradham, N. Basta, The bioavailability of chemicals in soil for earthworms, Ecotoxicol. Environ. Saf. 57 (2004) 39-47.

[4] D.M. Di Toro, H.E. Allen, H.L. Bergman, J.S. Meyer, P.R. Paquin, R.C. Santore, Biotic ligand model of the acute toxicity of metals. 1. Technical basis, Environ. Toxicol. Chem. 20 (2001) 2383-2396.

[5] P.R. Paquin, J.W. Gorsuch, S. Apte, G.E. Batley, K.C. Bowles, P.G.C. Campbell, C.G.. Delos, D.M. Di Toro, R.L. Dwyer, F. Galvez, R.W. Gensemer, G.G. Goss, C. Hogstrand, C.R. Janssen, J.C. McGeer, R.B. Naddy, R.C. Playle, R.C. Santore, U. Schneider, W.A. Stubblefield, C.M. Wood, K.B. Wu, The biotic ligand model: A historical overview, Comp. Biochem. Physiol. 133C (2002) 3-35.

[6] C.A.M. Van Gestel, J.E. Koolhaas, Water-extractability, free ion activity, and pH explain cadmium sorption and toxicity to *Folsomia candida* (collembola) in seven soil-pH combinations, Environ. Toxicol. Chem. 23 (2004) 1822-1833.

[7] S. Thakali, H.E. Allen, D.M. Di Toro, A.A. Ponizovsky, C.P. Rodney, F.J.

Zhao, S.P. McGrath, A Terrestrial Biotic Ligand Model. 1. Development and application to Cu and Ni toxicities to barley root elongation in soils, Environ. Sci. Technol. 40 (2006) 7085-7093.

[8] M. Koster, A. de Groot, M. Vijver, W. Peijnenburg, Copper in the terrestrial environment: Verification of a laboratory-derived terrestrial biotic ligand model to predict earthworm mortality with toxicity observed in field soils, Soil Biol. Biochem. 38 (2006) 1788-1796.

[9] B.K. Mandal, K.T. Suzuki, Arsenic round the world: a review, Talanta 58 (2002) 201-235.

[10] P.L. Smedley, D.G. Kinniburgh, A review of the source, behaviour and distribution of arsenic in natural waters, Appl. Geochem. 17 (2002) 517-568.

[11] D. Das, G. Samanta, B.K. Mandal, T.R. Chowdhury, C.R. Chanda, P.P. Chowdhury, G.K. Basu, D. Chakraborti, Arsenic in groundwater in six districts of West Bengal, India, Environ. Geochem. Health 18 (1996) 5-15.

[12] J. Susaya, K.-H. Kim, M.C. Jung, The impact of mining activities in alteration of As levels in the surrounding ecosystems: An encompassing risk assessment and evaluation of remediation strategies, J. Hazard. Mater. 182 (2010) 427-438.

[13] C.C. Tanner, J.S. Clayton, Persistence of arsenic 24 years after sodium arsenite herbicide application to Lake Rotoroa, Hamilton, New Zealand, New Zeal. J. Mar. Fresh. 24 (1990) 173-178.

[14] K.A.C. De Schamphelaere, C. R. Janssen, A biotic ligand model predicting acute copper toxicity for *Daphnia magna*: The effects of calcium, magnesium, sodium, potassium, and pH, Environ. Sci. Technol. 36 (2002)

48-54.

[15] R.S. Carr, M. Nipper, Porewater Toxicity Testing: Biological, Chemical, and Ecological Considerations, SETAC press, Pensacola, FL, USA, 2003.

[16] B.S. Anderson, J.W. Hunt, B.M. Phillips, R. Fairey, C.A. Roberts, J.M. Oakden, H.M. Puckett, M. Stephenson, R.S. Tjeerdema, E.R. Long, C.J. Wilson, J.M. Lyons, Sediment quality in Los Angeles harbor: A triad assessment, Environ. Toxicol. Chem. 20 (2001) 359-370.

[17] J.W. Hunt, B.S. Anderson, B.M. Phillips, J. Newman, R.S. Tjeerdema, M. Stephenson, H.M. Puckett, R. Fairey, R.W. Smith, K. Taberski, Evaluation and use of sediment reference sites and toxicity tests in San Francisco Bay. Sacramento CA, USA: State Water Resources Control Board. Bay Protection and Toxic Cleanup Program final technical report, 1998.

[18] J. An, S. Jeong, H.S. Moon, E.H. Jho, K. Nam, Prediction of Cd and Pb toxicity to Vibrio fischeri using biotic ligand-based models in soil, J. Hazard. Mater. 203-204 (2012) 69-76.

[19] C.N. Mulligan, R.N. Yong, B.F. Gibbs, An evaluation of technologies for the heavy metal remediation of dredged sediments, J. Hazard. Mater. 85 (2001) 145-163.

[20] S. Lee, J. An, Y.-J. Kim, K. Nam, Binding strength-associated toxicity reduction by birnessite and hydroxyapatite in Pb and Cd contaminated sediments, J. Hazard. Mater. 186 (2011) 2117-2122.

[21] USEPA. (2012). Solidification, from contaminated sites clean-up information (URL: http://www.cluin.org). Accessed Sep. 01, 2017.

[22] Z.D. Nejad, M.C. Jung, K.-H. Kim, Remediation of soils contaminated with heavy metals with an emphasis on immobilization technology, Environ. Geochem. Health (2017) DOI: 10.1007/s10653-017-9964-z.

CHAPTER 2

Evaluation of the Effectiveness of *In Situ* Stabilization in the Field Aged Arsenic-Contaminated Soil : Chemical Extractability and Biological Responses

2.1. Introduction

In situ stabilization of soils and sediments contaminated with metals and/or metalloids has been proposed due to concerns about disturbance to their ecosystems [1-3]. The mobility of metals and metalloids in soil can be alleviated by amending an appropriate sorbent that makes their chemical forms more stable via sorption and/or precipitation, thereby decreasing bioavailability and toxicity [3]. It can be effectively applied in areas where it might be difficult to carry out *ex situ* treatment that requires excavation and site closure [4].

Arsenic (As) contamination in the vicinity of an abandoned smelter in South Korea has been garnering attention due to its adverse effects on humans and surrounding ecosystem. Nonferrous metal smelting took place from 1936 to 1989 [5], and the As contamination of the surrounding soils has occurred through various sources, including arsenic trioxide (As_2O_3) emitted from the smelting stack, dust associated with ores (e.g., lead and copper ores containing arsenopyrite (FeAsS) and

arsenic sulfide (As_2S_3)), and field-disposed sludge produced from the smelting activity [4,5]. As concentrations in surface soils within 1.5 km from the smelting stack was found to frequently exceed the Korean soil regulatory levels for As (25 mg/kg for a rice paddy field, farmland, residential area, school, or park; 50 mg/kg for a forest, commercial area, or recreational area) [5]. Hence, the Korean government purchased the area to apply soil remedial actions. Some forest lands in the purchased area have limitations in carrying out *ex situ* treatments such as soil washing because preserving vegetation is important given the present land use as a tourist site [4]. In this respect, appropriate measures, such as *in situ* stabilization, must be carried out at this site to manage human health risk and ecotoxicity.

A variety of sorbents are reported to be capable of stabilizing As in soil [6]. Among them, iron (Fe) oxides such as ferrihydrite, goethite, hematite, and magnetite have been recognized for several decades as efficient stabilizing agents for As-contaminated soils [7,8]. By forming the outer- and/or inner-sphere complexes between the positively charged surface of Fe oxides and pentavalent arsenate ($HAsO_4^{2-}$ and $H_2AsO_4^-$) in soil porewater [9,10], the amendment of Fe oxides renders As in soil stable.

For *in situ* stabilization to be a valid risk mitigation measure, the stabilized As in soil should be chemically and biologically stable [1]. Since *in situ* stabilization does not physically remove As from soil, but retains it strongly bound, issues regarding the human health risk and ecotoxicity of the stabilized As in soil are critical. This study evaluated the effectiveness of *in situ* stabilization of the historically long-term As-contaminated soil in the vicinity of an abandoned smelter in South Korea by

means of (i) chemical extractability and the corresponding human health risk, and (ii) ecotoxicity to barley *Hordeum vulgare* as an indicator of biological responses. *In situ* stabilization was performed through the amendment of a Fe-based sorbent. To elucidate why chemical extractability and biological responses have changed, the X-ray absorption spectroscopy with the aid of linear combination fitting (LCF), and the analysis of soil physicochemical properties were performed.

2.2. Materials and methods

2.2.1. *In situ* stabilization

In situ stabilization at the forest near the old abandoned smelter in South Korea (longitude: 126°39’59.40’’, latitude: 36°00’27.46’’) was performed as follows: (i) pH adjustment, (ii) sorbent amendment, (iii) water spraying, and (iv) reaction for one week (April 3-10, 2017) (Figure 2.1). Because this site is covered with vegetation, and because the preservation of vegetation is important according to the land use as a sightseeing site, the application of *ex situ* treatments is limited [4]. First, the humus in the surface soil of a field experimental site (3 m width × 3 m length) was removed, and calcium oxide (CaO) was added to adjust the acidic soil pH to neutral levels (6 to 8). Our preliminary tests showed that neutralization of soil pH was possible when CaO was added to the soil at a weight of 0.14%. Second, the commercially available Fe-based sorbent was added to the soil at a weight of 1% based on a preliminary lab-scale test result [4]. The sorbent consists of 46.1% Fe_2O_3, 15.4% MgO, 14.3% CaO,

12.9% SO_3, 8.3% SiO_2, and 1.7% Al_2O_3, determined using X-ray fluorescence spectrometry (XRF) [4].

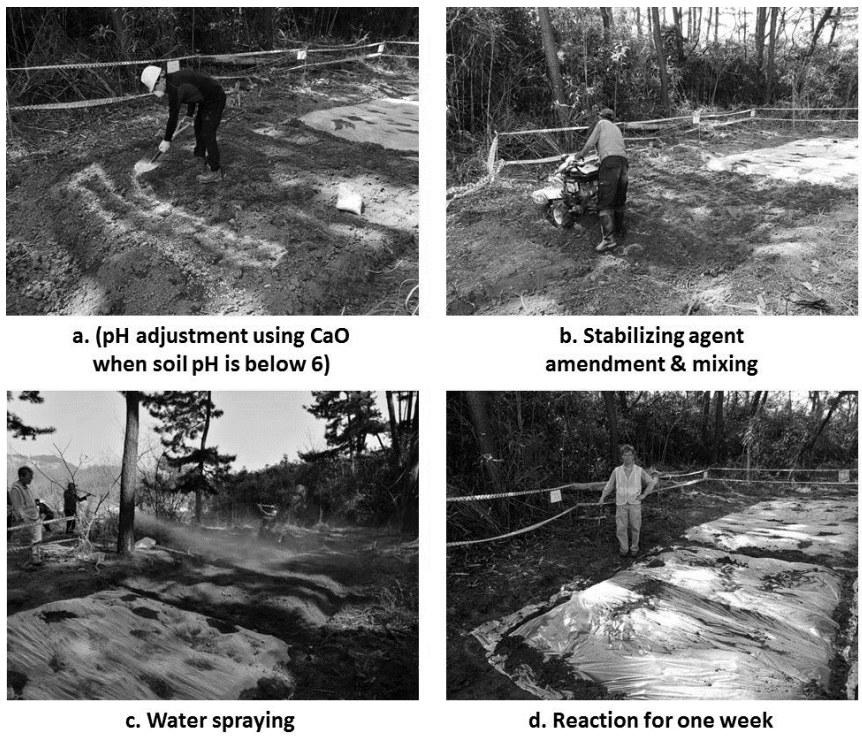

Figure 2.1. Procedure for application of stabilizing agents in As-contaminated soil at the forest area near an abandoned smelter site

The sorbent includes various Fe minerals, such as crystalline hematite, $FeSO_4$, $Fe_2(SO_4)_3$, and zero valent iron (ZVI), and dolomite ($CaMg(CO_3)_2$) [4]. A leachability test using a synthetic precipitation leaching procedure (SPLP) showed that As, Cd, Cr^{6+}, CN, Hg, Pb, organo-phosphorus, phenol, trichloroethylene, tetrachloroethylene, 1,1,1-Trichloroethane, benzene, toluene, ethylbenzene, and xylenes were not eluted above the limit of detection from the sorbent [4]. Third,

water was sprayed to adjust soil water content to field capacity (water corresponding to 33.4% of soil weight), and the surface soil was homogenized using a tractor. Finally, the soil was covered with vinyl so that rainwater would not enter, and the reaction proceeded for one week. Soil samples before and after *in situ* stabilization were collected from each 1 m width × 1 m length of the experimental site, and were mixed to attain homogeneity for future analysis. Each soil sample was air-dried and passed through a 2-mm sieve to remove debris and gravel, and stored at room temperature in dark condition.

2.2.2. Chemical extractability and human health risk characterization

2.2.2.1. Total As concentration in soil

The *aqua regia* digestion method was used to determine total As concentration in soil [11]. Three grams of soil passed through a 150-μm sieve after grinding (Gyral grinder, Chemplex, Stuart, FL, USA) were added to 21 mL HCl and 7 mL HNO_3 in a 100-mL Teflon vessel, then reacted for 2 h at 105°C using a heating block. The supernatant was filtered through a 0.45-μm GHP syringe filter (Pall Corporation, Port Washington, NY, USA) for As analysis. The As concentrations in the digested solutions were determined using inductively coupled plasma optical emission spectrometer (ICP-OES, iCAP7000 Series, Thermo Scientific, USA).

2.2.2.2. Bioaccessible As concentration in soil

The solubility bioavailability research consortium (SBRC) method was used to

calculate the in vitro bioaccessibility (IVBA) [12]. Briefly, 100 mL of 0.4 M glycine with pH 1.5 adjusted using concentrated HCl and 1 g of soil passed through a 150-μm sieve was reacted for 1 h in a 125-mL HDPE bottle at 37°C using a water bath. Then, the supernatant was filtered through a 0.45-μm GHP filter for As analysis. The As concentration in the extracted solution was determined using the ICP-OES.

2.2.2.3. Human health risk characterization through oral ingestion

According to Korean Soil Contaminant Risk Assessment Guidance [13], the human health risk of As through oral ingestion was determined assuming that the study site was used for residential purposes [5]. The average daily dose calculated using Eq. 2.1 was multiplied by slope factor to estimate the carcinogenic risk of As (Eq. 2.2) and divided by the reference dose to estimate the noncarcinogenic risk of As (Eq. 2.3):

$$ADD = \frac{C_S \times IVBA \times IR \times EF \times ED \times CF}{BW \times AT} \quad (2.1)$$

$$CR = ADD \times SF_{oral} \quad (2.2)$$

$$HQ = \frac{ADD}{RfD_{oral}} \quad (2.3)$$

where ADD is the average daily dose (mg/kg-day), C_s is the total concentration of As in soil through *aqua regia* digestion (mg/kg), IVBA is the in vitro bioaccessibility

(i.e., SBRC-extractable As concentration in soil divided by total As concentration in soil), IR is the ingestion rate of soil (50 mg/day for adults, 118 mg/day for children), EF is the exposure frequency (350 days/year for both adults and children), ED is the exposure duration (25 years for adults and 6 years for children), CF is a unit conversion factor (10^6 kg/mg), BW is the body weight (62.8 kg for adults and 16.8 kg for children), AT is the averaging time (carcinogen: 28,689 days for both adults and children, noncarcinogen: 9,125 days for adults and 2,190 days for children), CR is the carcinogenic risk, SF_{oral} is the oral slope factor (1.5 kg-day/mg), HQ is the noncarcinogenic risk (hazard quotient; HQ), and RfD_{oral} is the oral reference dose (3.0×10^4 mg/kg-day) [5].

2.2.2.4. Five step sequential extraction

A sequential extraction proposed by Wenzel et al. [14] was used to investigate chemical forms of As in soil after *in situ* stabilization. The sequential extraction method differentiates chemical forms of As in soil into five fractions as follows: (i) F1: nonspecifically bound As ($(NH_4)_2SO_4$ extractable), (ii) F2: specifically bound As ($(NH_4)H_2PO_4$ extractable), (iii) F3: amorphous iron oxides bound As (NH_4-oxlatate extractable), (iv) F4: crystalline iron oxides bound As (NH_4-oxalate/ascorbic acid extractable), and (v) F5: residual As. In the present study, F5 was determined using the USEPA 3052 method [15]. The As concentrations in the extracted solutions were determined using ICP-OES after performing the filtration using a 0.45-μm GHP filter.

2.2.3. Ecotoxicity test with *H. vulgare* as an indicator of biological responses

The growth of barley (*H. vulgare*), measured via germination rate, root elongation, and shoot elongation was assessed to compare the ecotoxicity in soil before and after *in situ* stabilization. Seeds were sterilized with a 5% NaOCl solution (Daejung, Korea) for 10 min, rinsed three times with deionized (DI) water, then exposed on a wet cotton surface for 3 h [16]. Then, five seeds were placed in each soil sample (50 g) within a 100-mL polyethylene vial. Water was added to reach the field capacity of the soil (water corresponding to 33.4% of soil dry weight). Each vial was incubated under constant conditions (20°C in a 16:8 light:dark photoperiod) using a growth chamber (E15, Conviron, Canada). The germination rate and root and shoot elongations were measured after 5 d.

2.2.4. X-ray absorption spectroscopy

To assess Fe oxide distribution in soil after *in situ* stabilization (i.e., to understand the form of the amended sorbent in soil), Fe K-edge X-ray absorption near edge structure (XANES) spectra obtained from the beamline 7D at the Pohang Accelerator Laboratory (PAL) in South Korea were used with the aid of LCF. The spectra were produced in transmittance mode using Fe foil as a reference. The ATHENA program was used to process raw spectra (i.e., spectral averaging, normalization of edge-step, and background removal) [17]. For LCF analysis, edge-normalized spectra of ferrihydrite ($(Fe^{3+})_2O_3 \cdot 0.5H_2O$), hematite (α-Fe2O3), goethite (α-FeOOH), schwertmannite ($Fe_8O_8(OH)_6(SO_4) \cdot nH_2O$), and wustite (FeO) were used as predictor components. The goodness of fitness was evaluated using R-factor and reduced χ^2

[18]. The R-factor and the reduced χ^2 are the sum of the squares of the difference between the fit and the data and the fitting metric divided by the number of degrees of freedom, respectively [18]. Distribution of Fe oxides in the soil can be qualitatively and quantitatively assessed through a combination of predictors that make both the R-factor and the reduced χ^2 the smallest. To confirm the valence of As in soil, As K-edge XANES spectra collected from the beamline 7D at the PAL using the fluorescence mode with Na_2HAsO_4 as a reference were used.

2.2.5. Soil physicochemical properties

Soil pH, texture, cation exchange capacity (CEC), organic matter (OM) content, Fe/Al/Mn oxides concentrations, available phosphorus (P_2O_5) concentration, and exchangeable cation (Ca^{2+}, Mg^{2+}, K^+, and Na^+) concentrations were assessed [19-24] to investigate the effect of *in situ* stabilization on the soil physicochemical properties. In addition, the content of major constituents in the soil was determined using XRF. Crystalline minerals in the soil were identified using an X-ray diffractometer (XRD) with Cu-Kα radiation operated at 40 kV and 40 mA, and the scanning range was between 5 and 90°.

2.3. Results and discussion

2.3.1. Chemical extractability and human health risk

Total As concentrations in the original and stabilized soils were 142 and 152 ± 9 mg/kg, respectively (Table 2.1). Since stabilization process is a kind of risk reduction, not concentration reduction, it is noteworthy that SBRC-extractable As concentrations slightly decreased after *in situ* stabilization. Since the adsorbed As in the Fe-based sorbent is resistant to SBRC extraction, the SBRC-extractable As concentration decreased from 16.0 to 13.0 ± 0.2 mg/kg (Table 2.1).

Table 2.1. Total As concentration in soil determined using *aqua regia* digestion method and the SBRC-extractable As concentration in soil, and carcinogenic risk and noncarcinogenic risk through oral ingestion after in situ stabilization

In situ stabilization	Total As concentration (mg/kg)	SBRC-extractable As concentration (mg/kg)	Carcinogenic risk (CR)[a]	Noncarcinogenic risk (HQ)[a]
Before	142	16.0	1.21E-05	0.352
After	152 ± 9	13.0 ± 0.2	1.02E-05	0.296

[a]All risks calculated in Table 2.1 are values for children because they are higher than those for adults (thus, a more conservative assessment).

Yang et al. [25] observed that the SBRC-extractable As concentration decreased when magnetite was amended in soil samples, similar to the results of this study. The

SBRC-extractable As is more likely to be bioavailable and pose potential risk, and thus often be used for in vitro bioaccessibility (IVBA) calculation. Human health risks through oral ingestion after *in situ* stabilization in As-contaminated soil are estimated with considering IVBA. The carcinogenic risk (CR) and noncarcinogenic risk (HQ) after *in situ* stabilization decreased from 1.21E-05 to 1.02E-05 and 0.352 to 0.296, respectively (Table 2.1).

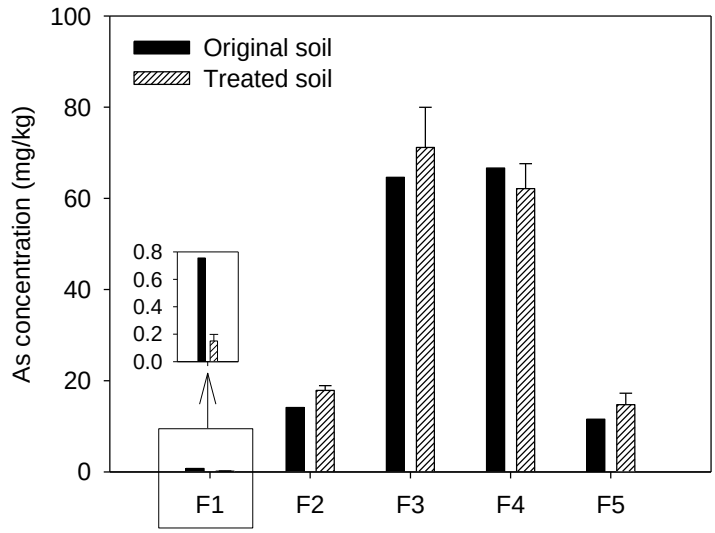

Figure 2.2. Chemical forms of As determined by Wenzel's sequential extraction method after in situ stabilization. Soil-bound As was divided into five fractions, as follows: F1 (nonspecifically bound As), F2 (specifically bound As), F3 (As associated with amorphous Fe/Al oxides), F4 (As associated with crystalline Fe/Al oxides), and F5 (residual As). Error bars indicate the standard deviation (n = 3).

Chemical forms of As in soil determined using the five step sequential extraction by Wenzel [14] after *in situ* stabilization are shown in Figure 2.2. Nonspecifically bound As in soil (F1) dramatically decreased from 0.76 to 0.15 ± 0.05 mg/kg, while

other fractions did not noticeably change (Figure 2.2). This portion of As in soil can readily migrate to soil porewater and therefore appears to be bioavailable, and it freely transfers from soil to plants.

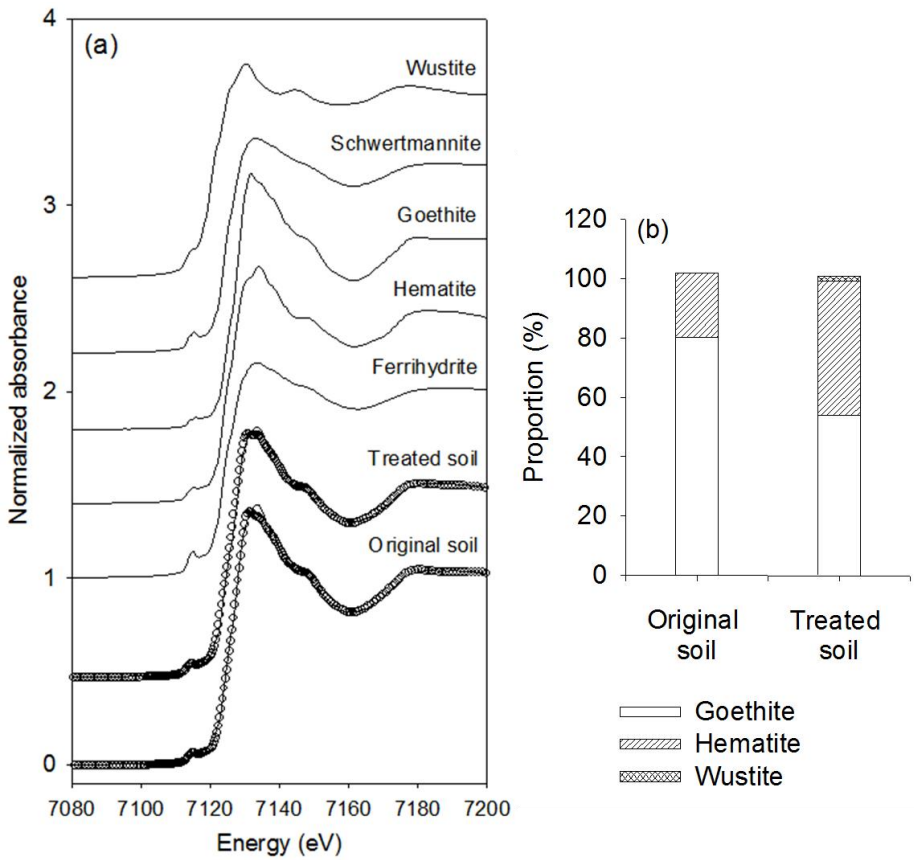

Figure 2.3. Fe K-edge XANES spectra (solid lines) of ferrihydrite, hematite, goethite, schwertmannite, wustite, original soil, and stabilized soil and linear combination fitting (LCF) results (open circles) of the original soil and the stabilized soil (a). The goodness of fit was 0.0015 for R-factor and 0.0003 for reduced χ^2 in the original soil and 0.0005 for R-factor and 0.0001 for reduced χ^2 in the stabilized soil, respectively. The stacked column graph shows the proportion of model compounds (five different Fe oxides) for the sample spectrum (b).

To assess the possible stabilization mechanism of As, Fe K-edge XANES spectra of soils before and after *in situ* stabilization were compared with the XANES spectra of several Fe minerals (i.e., ferrihydrite, hematite, goethite, schwertmannite, and wustite). The LCF of XANES spectra for Fe minerals was able to efficiently estimate the XANES spectrum of the soil (Figure 2.3a), and the proportion of Fe minerals consisting of Fe in the soil is shown in Figure 2.3b. The goodness of fitness is described by an R-factor of 0.0015 and a reduced χ^2 of 0.0003 in the original soil, and 0.0005 and 0.0001 in the stabilized soil, respectively. The original soil mainly consisted of goethite (80%) and hematite (20%), and the stabilized soil consisted of goethite (54.3%), hematite (45.5%), and wustite (0.2%) (Figure 2.3b). The LCF result indicates that some of the goethite in the original soil and Fe minerals in the sorbent (i.e., $FeSO_4$, $Fe_2(SO_4)_3$, and ZVI) were converted to hematite. In previous studies, Murray et al. [26] reported that the transformation of goethite into hematite can be accelerated at higher caustic concentrations or temperatures. Das et al. [27] observed that two-line ferrihydrite converts to hematite through a two-phase crystalline process with intermediate goethite. Cudennec and Lecerf [28] confirmed that the formation of hematite from ferrihydrite is favored at neutral pH (values around 7) while obtaining goethite is favored at low and high values of pH (2 to 5 and 10 to 14). Overall, the change in pH from acidic to neutral under oxic conditions, the formation of hematite in the soil can be facilitated. Maximum adsorption capacities of hematite for iAs(V) and iAs(III) are higher than goethite [8]. It is reasonable to describe that the formation of hematite in the stabilized soil could occur because the soil pH increased from 4.6 to 6.9 (Table 2.2) after the neutralization for *in situ* stabilization in this study, and the hematite newly formed might adsorb As in

the soil.

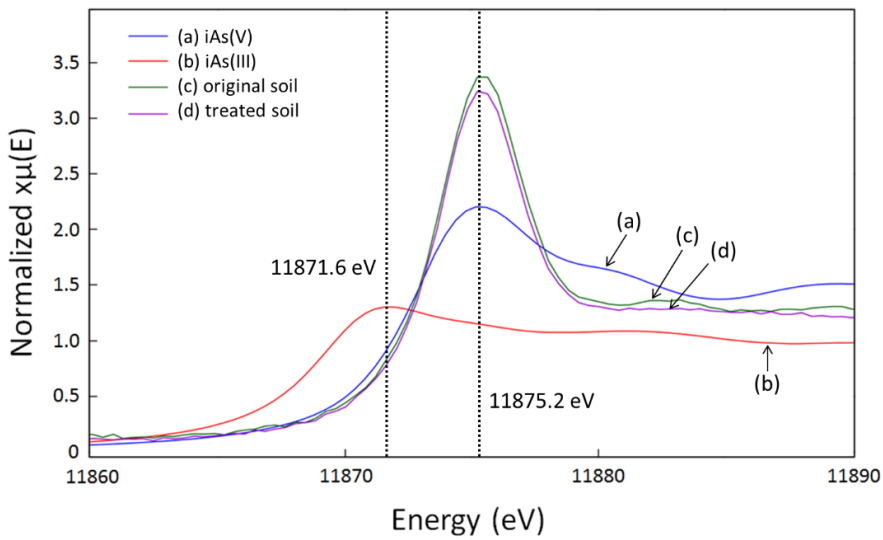

Figure 2.4. As K-edge XANES spectra of (a) inorganic pentavalent arsenate (iAs(V)) model compound, (b) inorganic trivalent arsenite (iAs(III)) model compound, (c) original soil (i.e., As-contaminated soil), and (d) stabilized soil (i.e., As-contaminated soil after in situ stabilization). The peaks of iAs(V), the original soil, and the stabilized soil appeared at 11875.2 eV, while the peak of iAs(III) appeared at 11871.6 eV.

Interestingly, Fe oxide concentrations measured using the dithionite-citrate system buffered with sodium bicarbonate (DCB) method [23] decreased from 20,777 to 18,462 mg/kg, although total Fe content determined using XRF increased (Table 2.2). The fact that the DCB method does not always result in a complete dissolution of Fe oxides has been shown [29,30]. Ryan and Gschwend [30] observed that hematite was dissolved to 62% after DCB treatment, while 87% of the goethite was dissolved. The decrease of Fe oxide content determined by the DCB method supports the fact that hematite was formed in the stabilized soil.

The oxidation state of As in soil was determined using As K-edge XANES analysis. The XANES spectra of $NaAsO_2$ and Na_2HAsO_4 dissolved in DI water were used as references for trivalent inorganic arsenite (iAs(III)) and pentavalent inorganic arsenate (iAs(V)), respectively. The XANES spectra of the original and the stabilized soils showed an absorption edge energy at 11,875.2 eV, while those of iAs(III) and iAs(V) were observed at 11,871.6 and 11,875.2 eV (Figure 2.4). In general, the oxidation of ZVI and Fe(II) (i.e., components of the sorbent) to Fe(III) can proceed the reduction of iAs(V) to iAs(III), thereby forming arsenopyrite (FeAsS) [31]. However, the fact that the oxidation state of As in soil was +5 regardless of whether or not the Fe-based sorbent was amended in the soil demonstrates the formation of arsenopyrite does not occur.

As a consequence, the hematite newly transformed from goethite in soil and from $FeSO_4$, $Fe_2(SO_4)_3$, and ZVI in the Fe-based sorbent seems to adsorb labile As present in soil, thereby lowering the SBRC-extractable As concentration and nonspecifically bound As in five step sequential extraction.

2.3.2. Biological responses

The shoot elongation of *H. vulgare* was significantly lower in the stabilized soil than in the original soil (Figure 2.5). Although the germination rate and root elongation of *H. vulgare* also decreased, these changes were not statistically significant ($p > 0.05$). The lower growth of *H. vulgare* in the stabilized soil than in the original soil cannot be explained by the decrease of the nonspecifically bound As concentration in soil, suggesting that other factors may exhibit a stronger relationship

with ecotoxicological responses [32,33].

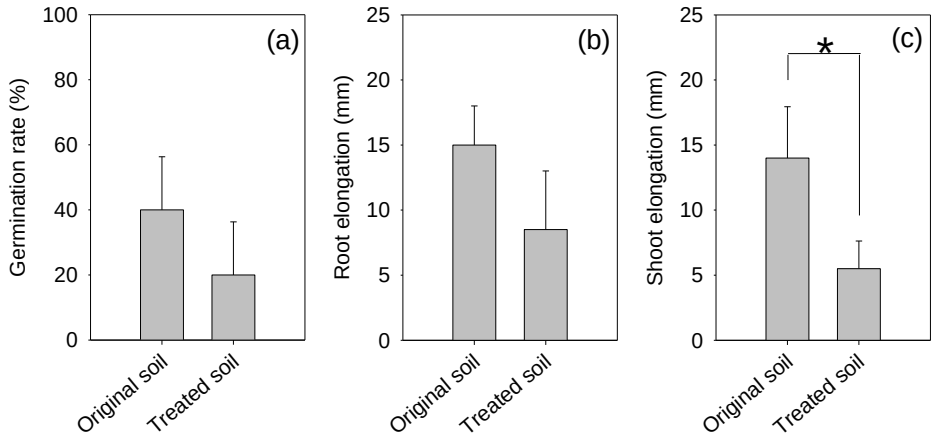

Figure 2.5. Effect of in situ stabilization on (a) seed germination of barley (*H. vulgare*), (b) root elongation, and (c) shoot elongation. Error bars represent the standard deviation. The asterisk indicates a significant difference ($p < 0.05$) between two groups from a Student's *t*-test.

It is noteworthy that the available phosphorus concentration in the soil significantly decreased from 60.2 to 13.8 mg/kg (Table 2.2), both of which are lower than the recommended available phosphorus concentration range for agricultural soils in South Korea of 80 to 550 mg/kg [34]. Phosphorus deficiency (a.k.a. starvation) can impose an oxidative stress in root cells [35]. Hence, the adsorption of available phosphorus to positively charged Fe oxides newly formed in the stabilized soil (e.g, hematite) seems to be one of the reasons for the lowered growth of *H. vulgare*. In addition, following Lamb et al. [36] and Wang et al. [37], iAs(V) toxicity can be alleviated by the presence of phosphate through a competition effect. This phenomenon originates from the similarity of chemical structures between

phosphate and arsenate, and modes of toxic action of iAs(V) can be inhibited by phosphate, and this similarity is often used to extract As from soil [38].

Table 2.2. Soil physicochemical properties after *in situ* stabilization

Soil physicochemical property		*In situ* stabilization (sorbent amendment)	
		Before	After
pH		4.6	6.9
Organic matter (%)		8.5	4.9
Cation exchange capacity (cmol/kg)		23.6	24.3
Texture (%)	Sand	40.4	34.1
	Silt	29.7	36.3
	Clay	29.9	29.6
	Classification	Clay loam	Clay loam
Major constituents (%)[a]	SiO_2	42.2	40.7
	Al_2O_3	17.3	16.2
	Fe_2O_3	6.8	8.3
	K_2O	1.7	1.7
	MgO	0.83	0.82
	TiO_2	0.82	0.84
	Na_2O	0.34	0.33
	CaO	0.31	1.2
	SO_3	0.19	0.39
	P_2O_5	0.18	0.16
	MnO	0.07	0.06
	PbO	0.06	0.06
	As_2O_3	0.02	0.02
Oxide content (mg/kg)[b]	Fe oxides	20777	18462
	Al oxides	1156	1485

	Mn oxides	158	171
Exchangeable cations (mg/kg)	Ca^{2+}	593	3142
	Mg^{2+}	95.0	84.1
	K^{+}	95.4	86.6
	Na^{+}	11.2	12.6
Available phosphorus (P_2O_5) (mg/kg)		60.2	13.8
Crystalline compounds[c,d]		Quartz (67.9%) Muscovite (18.4%) Albite (9.0%) Kaolinite (4.1%)	Quartz (65.7%) Muscovite (12.9%) Albite (17.4%) Kaolinite (3.6%)

[a]The content of major constituents was determined using XRF.

[b]Contents of Fe/Al/Mn oxides were measured using the DCB method.

[c]Crystalline compounds were determined using XRD and the values in parentheses refers to the semi-quantitative analysis values obtained from the XRD analysis, which means the relative proportion of the crystalline compounds.

[d]Quartz = SiO_2, Muscovite = $K(Al_{0.876}Fe_{0.124})_2Fe_{0.067}(Si_{1.64}Al_{0.36})_2O_{10}((OH)_{0.914}F_{0.086})_2$, Albite = $Na_{0.98}Ca_{0.02}Al_{1.02}Si_{2.98}O_8$, and Kaolinite = $Al_2Si_2O_5(OH)_4$

Exchangeable Ca^{2+} concentrations in soil after *in situ* stabilization significantly increased, from 593 to 3,142 mg/kg (Table 2.2), owing to the addition of CaO for adjusting soil pH. This is likely to affect the increase in iAs(V) toxicity to *H. vulgare* through a change in membrane potential. Wang et al. [39] observed that a significant increase of iAs(V) toxicity to wheat (*Triticum aestivum*) as increased Ca^{2+} activity in bulk solution. This can be attributed to the fact that an increase in Ca^{2+} activity from 0.2 to 2.5 mM in bulk solution increases the membrane surface potential from -40 to -20 mV, resulting in a higher accumulation of $H_2AsO_4^-$ and $HAsO_4^{2-}$ onto the cell membrane surface of *T. aestivum* and an increase in toxicity [39]. Because barley

is a salt-tolerant plant, osmotic stress from an increase in exchangeable Ca^{2+} is not likely to occur (threshold electrical conductivity of barley = 8 dS/m) [40].

2.4. Summary

In situ stabilization as a risk mitigation measure was performed in historically long-term As-contaminated soil in the vicinity of an abandoned smelter via the amendment with the Fe-based sorbent. The effectiveness of *in situ* stabilization was assessed by means of chemical extractability and biological responses. Chemical extractability of As in soil determined using SBRC extraction slightly decreased, thereby lowering the human health risk through oral ingestion. Nonspecifically bound As in soil determined using five step sequential extraction also significantly decreased. These might be due to a formation of hematite that can adsorb As in soil according to the amendment of the Fe-based sorbent with CaO for the neutralization. The shoot growth of *H. vulgare* significantly decreased, probably due to an increase in exchangeable Ca^{2+}, resulting in an accumulation of iAs(V) in the membrane surface of *H. vulgare*, and a decrease in available phosphorus, resulting in a decrease in competition between iAs(V) and phosphate, as well as phosphorus starvation. Overall, to ensure the effectiveness of *in situ* stabilization, chemical extractability as well as biological responses (ecotoxicity) should be continuously monitored, as chemical analysis alone is insufficient to assess the ecotoxicological responses of As in soil, as presented in this study.

References

[1] S. Lee, J. An, Y.-J. Kim, K. Nam, Binding strength-associated toxicity reduction by birnessite and hydroxyapatite in Pb and Cd contaminated sediments, J. Hazard. Mater. 186 (2011) 2117-2122.

[2] J.-F. Peng, Y.-H. Song, P. Yuan, X.-Y. Cui, G.-L. Qiu, The remediation of heavy metals contaminated sediment, J. Hazard. Mater. 161 (2009) 633-640.

[3] A. Chlopecka, D.C. Adriano, Mimicked in-situ stabilization of metals in a cropped soil: Bioavailability and chemical form of zinc, Environ. Sci. Technol. 30 (1996) 3294-3303.

[4] J. An, K. Yang, W. Kang, J.S. Lee, K. Nam, Risk mitigation measures in arsenic-contaminated soil at the forest area near the former Janghang smelter site: Applicability of stabilization technique and follow-up management plan, J. Soil Groundwater Environ. 22(6) (2017) 1-11. (in Korean)

[5] K. Yang, J. Im, S. Jeong, K. Nam, Determination of human health risk incorporating experimentally derived site-specific bioaccessibility of arsenic at an old abandoned smelter site, Environ. Res. 137 (2015) 78-84.

[6] D. Mohan, C.U. Pittman Jr, Arsenic removal from water/wastewater using adsorbents—A critical review, J. Hazard. Mater. 142 (2007) 1-53.

[7] A. Voegelin, S.J. Hug, Catalyzed oxidation of arsenic(III) by hydrogen peroxide on the surface of ferrihydrite: an *in situ* ATR-FTIR study, Environ.

Sci. Technol. 37 (2003) 972-978.

[8] J. Giménez, M. Martínez, J. de Pablo, M. Rovira, L. Duro, Arsenic sorption onto natural hematite, magnetite, and goethite. J. Hazard. Mater. 141 (2007) 575-580.

[9] K. Yang, B.-C. Kim, K. Nam, Y. Choi, The effect of arsenic chemical form and mixing regime of arsenic mass transfer from soil to magnetite, Environ. Sci. Pollut. Res. 24 (2017) 8479-8488.

[10] D.M. Sherman, S.R. Randall, Surface complexation of arsenic(V) to iron(III) (hydr)oxides: Structural mechanism from ab initio molecular geometries and EXAFS spectroscopy, Geochim. Cosmochim. Acta 67 (2003) 4223-4230.

[11] ISO (International Organization for Standardization), ISO 11466:1995 – Soil Quality – Extraction of Trace Elements Soluble in *Aqua Regia*, 1995.

[12] M.E. Kelly, S. Brauning, R. Schoof, M. Ruby, Assessing Oral Bioavailability of Metals in Soil, Battelle Press, Columbus, OH, USA, 2002.

[13] KMOE (Korea Ministry of Environment), Soil Contaminant Risk Assessment Guidance, Gwacheon, Republic of Korea, 2011.

[14] W.W. Wenzel, N. Kirchbaumer, T. Prohaska, G. Stingeder, E. Lombi, D.C. Adriano, Arsenic fractionation in soils using an improved sequential extraction procedure, Anal. Chim. Acta 436 (2001) 309-323.

[15] USEPA (United States Environmental Protection Agency), Method 3052 - Microwave Assisted Acid Digestion of Siliceous and Organically Based Matrices, 1996.

[16] Y. Chae, D. Kim, Y.-J. An, Effects of fluorine on crops, soil exoenzyme

activities, and earthworms in terrestrial ecosystems, Ecotoxicol. Environ. Saf. 151 (2018) 21-27.

[17] B. Ravel, M. Newville, ATHENA, ARTEMIS, HEPHAESTUS: Data analysis for X-ray absorption spectroscopy using IFEFFIT, J. Synchrotron Radiat. 12 (2005) 537-541.

[18] J.H. Park, Y.-S. Han, J.S. Ahn, Comparison of arsenic co-precipitation and adsorption by iron minerals and the mechanism of arsenic natural attenuation in a mine stream, Water Research 106 (2016) 295-303.

[19] G.W. Thomas, Soil pH and Soil Acidity, in: D.L. Sparks (Ed.), Methods of Soil Analysis: Part 3. Chemical Methods, Soil Science Society of America Inc., Madison, WI, USA, 1996.

[20] M.E. Sumner, W.P. Miller, Cation Exchange Capacity and Exchange Coefficients, in: D.L. Sparks (Ed.), Methods of Soil Analysis: Part 3. Chemical Methods, Soil Science Society of America Inc., Madison, WI, USA, 1996.

[21] G.W. Gee, J.W. Bauder, Particle-size Analysis, in: A. Klute (Ed.), Methods of Soil Analysis: Part 1. Physical and Mineralogical Methods, Soil Science Society of America Inc., Madison, WI, USA, 1986.

[22] A. Walkley, I.A. Black, An examination of the Degtjareff method for determining soil organic matter, and a proposed modification of the chromic acid titration method, Soil Sci. 37 (1934) 29–38.

[23] O. Mehra, M. Jackson, Iron oxide removal from soils and clays by a dithionite-citrate system buffered with sodium bicarbonate, Clays Clay Miner. 7 (1958) 317-327.

[24] R.H. Bray, L. Kurtz, Determination of total, organic, and available forms of phosphorus in soils. Soil Sci. 59 (1945) 39-46.

[25] K. Yang, B.-C. Kim, K. Nam, Y. Choi, The effect of arsenic chemical form and mixing regime on arsenic mass transfer from soil to magnetite, Environ. Sci. Pollut. Res. 24 (2017) 8479-8488.

[26] J. Murray, L. Kirwan, M. Loan, B.K. Hodnett, In-situ synchrotron diffraction study of the hydrothermal transformation of goethite to hematite in sodium aluminate solutions, Hydrometallurgy 95 (2009) 239-246.

[27] S. Das, M.J. Hendry, J. Essilfie-Dughan, Transformation of two-line ferrihydrite to goethite and hematite as a function of pH and temperature, Environ. Sci. Technol. 45 (2011) 268-275.

[28] Y. Cudennec, A. Lecerf, The transformation of ferrihydrite into goethite or hematite, revisited, J. Solid State Chem. 179 (2006) 716-722.

[29] O.K. Borggaard, Selective extraction of amorphous iron oxides by EDTA from selected silicates and mixtures of amorphous and crystalline iron oxides, Clay Miner. 17 (1982) 365-368.

[30] J.N. Ryan, P.M. Gschwend, Extraction of iron oxides from sediments using reductive dissolution by titanium(III), Clays Clay Miner. 39 (1991) 509-518.

[31] B.A. Manning, M.L. Hunt, C. Amrhein, J.A. Yarmoff, Arsenic(III) and arsenic(V) reactions with zerovalent iron corrosion products. Environ. Sci. Technol. 36 (2002) 5455-5465.

[32] Q.-Y. Wang, D.-M. Zhou, L. Cang, T.-R. Sun, Application of bioassays to evaluate a copper contaminated soil before and after a pilot-scale

electrokinetic remediation, Environ. Pollut. 157 (2009) 410-416.

[33] G. Plaza, G. Nat ęcz-Jawaki, K. Ulgih, R.L. Bridmon, The application of bioassays as indicators of petroleum-contaminated soil remediation, Chemosphere 59 (2005) 289-296.

[34] KSIS (Korean Soil Information System), 2015. Soil Composition. Rural Development Administration.

[35] I. Juszczuk, E. Malusà, A.M. Rychter, Oxidative stress during phosphate deficiency in roots of bean plants (*Phaseolus vulgaris* L.), J. Plant Physiol. 158 (2001) 1299-1305.

[36] D.T. Lamb, M. Kader, L. Wang, G. Choppala, M.M. Rahman, M. Megharaj, R. Naidu, Pore-water carbonate and phosphate as predictors of arsenate toxicity in soil, Environ. Sci. Technol. 50 (2016) 13062-13069.

[37] N.-X. Wang, Y. Li, X.-H. Deng, A.-J. Miao, R. Ji, L.-Y. Yang, Toxicity and bioaccumulation kinetics of arsenate in two freshwater green algae under different phosphate regimes, Water Res. 47 (2013) 2497-2506.

[38] J. Im, K. Yang, S. Moon, Y.-J. Kim, K. Nam, Role of phosphate and Fe-oxides on the acid-aided extraction efficiency and readsorption of As in field-aged soil, J. Hazard. Mat. 300 (2015) 161-166.

[39] P. Wang, D. Zhou, T.B. Kinraide, X. Luo, L. Li, D. Li, H. Zhang, Cell membrane surface potential (Ψ0) plays a dominant role in the phytotoxicity of copper and arsenate, Plant Physiol. 148 (2008) 2134-2143.

[40] D.L. Sparks, Environmental Soil Chemistry, Academic Press, San Diego, CA, USA, 1995.

CHAPTER 3

Extension of Biotic Ligand Model to Account for the Effects of pH and Phosphate in Accurate Prediction of Arsenate Toxicity

3.1. Introduction

Arsenic (As), a highly toxic metalloid, is found throughout the aquatic and terrestrial environments [1,2]. It originates from both natural sources including the weathering and/or dissolution of As-bearing minerals such as arsenopyrite (FeAsS) and orpiment (As_2S_3) [3] and anthropogenic sources such as mining activity, pesticides, and wood preservatives [4-6]. It also can exist in both inorganic and organic forms in four oxidation states (i.e., +V, +III, 0, and –III) [7,8]. Among them, pentavalent inorganic arsenate (iAs(V)) is the most stable and predominates in the oxidizing environmental conditions.

Evidence collected in the past decades showed that the total concentration of metals or metalloids is not a good indicator of ecotoxicity [9-12]. Several environmental factors in aquatic and terrestrial systems, such as pH, major cations and anions, and dissolved organic matter can significantly affect the bioavailability and toxicity of metals and metalloids [11,13-22]. As such, when toxicity prediction

models are employed, those components should be considered to determine the site-specific toxicity of metals and metalloids.

Biotic ligand model (BLM), a semi-mathematical and equilibrium model, has been proposed for the prediction of the toxicity of cationic metals by using site-specific water characteristics [9,10,23,24]. Once established, the model has a great advantage because it does not require site-specific toxicity assay. Instead, chemical analysis data of the site of interest is only needed. BLM assumes that the free metal ions in the body of water bind to the active binding sites (i.e., biotic ligand, BL) of an organism and that the fraction of BL occupied by free metal ions (*f*) can be directly attributed to the toxic effect [23,24]. Furthermore, major cations such as Ca^{2+}, Mg^{2+}, and H^{+} compete with free metal ions for the available BL sites, which change the *f* value. Even if the free metal ion concentrations (or activities) are the same, such competition diminishes the toxic effect of cationic metals [21,24,25]. This BLM approach has been successfully applied to predict the toxicity of Cd, Cu, Ni, Pb, and Zn [21,24,26,27].

Despite the extensive previous studies for cationic metals, application of the BLM approach to predict iAs(V) toxicity is very few. Rubinos et al. [11] and Wang et al. [28] investigated the effect of phosphate on iAs(V) toxicity, which presumably caused by the structural similarity between the two species, but the subsequent model development incorporating phosphate has not been reported. Although Chen et al. [29] and Tsai et al. [30] proposed the combination of BLM and damage assessment model to predict chronic iAs(V) toxicity to tilapia, the concept of BLM for cationic metals was used without modification (i.e., use of the binding affinity between major

cations and BL: K_{MgBL}, K_{CaBL}, K_{HBL}, and K_{NaBL}). Hence, the competition of major anions including phosphate to active binding sites on the cell membrane of organism with iAs(V), which are present as oxyanions ($HAsO_4^{2-}$, $H_2AsO_4^-$) in natural water systems, cannot reflect at all. Currently, the lack of BLM parameters for the competing ions is the biggest obstacles to apply the BLM approach to predict iAs(V) toxicity.

In this study, the effect of environmental factors including pH, major cations (Ca^{2+}, Mg^{2+}, and K^+), and major anions ($HPO_4^{2-}/H_2PO_4^-$, SO_4^{2-}, NO_3^-, and HCO_3^-) on the toxicity of iAs(V), one of the most abundant As species in natural water systems, to the bioluminescence bacterium *Aliivibrio fischeri* was systematically investigated. A toxicity prediction model for iAs(V) was developed by reconstructing the existing BLM with incorporating the effects of pH and phosphate. Specifically, the parameters for a predictive model of iAs(V) toxicity (i.e., K_{XHAsO4}, $K_{XH2AsO4}$, K_{XHPO4}, K_{XH2PO4}, $f_{mix}^{50\%}$) were determined.

3.2. Materials and methods

3.2.1. Toxicity test

The toxicity of iAs(V) was assessed by using a bioluminescent bacterium, which was recently renamed from *Vibrio fischeri* to *A. fischeri* [31]. The light production from *A. fischeri* was detected by using a Microtox® 500 analyzer (SDI, Carlsbad, CA) and diminishes in the presence of toxic substances. The toxicity of iAs(V) (i.e.,

the bioluminescence inhibition) after exposure to a given concentration of contaminant for 5 min was calculated from Eq. 3.1.

$$R = (1 - \frac{I_t}{I_0 C_t}) \times 100 \quad (3.1)$$

where R is the bioluminescence inhibition (toxic effect) in *A. fischeri*, C_t is the correction factor obtained when the light intensity of the control remaining after 5 min is divided by the initial light intensity of the control, I_t is the light intensity of the test sample after 5 min, and I_o is the initial light intensity of the sample [32].

The changes in the bioluminescence inhibition in response to changes in iAs(V) concentrations or activities were fitted by sigmoidal dose-response curves to calculate EC50 values (i.e., the iAs(V) concentration or activity that resulted in 50% inhibition of the light production from *A. fischeri*) [21,33].

3.2.2. Reagents and sample preparation

All reagents used in this study were of analytical grade. Deionized (DI) water, with a resistance of 18.2 MΩ cm (Milli-Q, Millipore, Bedford, MA), was used throughout. A stock solution of iAs(V) (0.1 M) was prepared by dissolving $Na_2HAsO_4 \cdot 7H_2O$ (98.0%–102%, Sigma-Aldrich) in DI water and stored in the dark at 4 °C. To adjust the pH of the tested solution, 2-[N-morpholino] ethane sulfonic

acid (MES, Sigma), 3-[N-morpholino] propanesulfonic acid (MOPS, > 99.5%, Sigma), and tris[hydroxymethyl] aminomethane (Tris, > 99.8%, Sigma-Aldrich) buffering solutions were used. To assess the effect of major cations or anions on iAs(V) toxicity, $CaCl_2 \cdot 2H_2O$ (> 98%), $MgCl_2 \cdot 6H_2O$ (> 98%), KCl (> 99%), Na_2HPO_4 (> 98%), $NaHCO_3$ (99.0%–100.5%), Na_2SO_4 (> 99%), and $NaNO_3$ (> 99%), all purchased from Daejung (Korea), were used. The HA (Elliott soil humic acid standard IV) was purchased from International Humic Substances Society (IHSS). The elemental composition of HA was follows: 59.5% carbon, 3.2% hydrogen, 32.2% oxygen, 3.9% nitrogen, 0.47% sulfur, and 0.44% ash [46].

3.2.3. Effect of pH on iAs(V) toxicity

In order to investigate the effect of pH on iAs(V) toxicity, toxicity assays were conducted in different pH solutions (5, 6, 6.5, 7, 7,5, 8, 8.5, and 9). Each test used the Extended (9 dilution) Test Method [32]. The concentrations of iAs(V) in solution of test medium (i.e., the concentration in direct contact with *A. fischeri*) were in the range from 5 μM to 50 mM. The pH values were controlled at 5–6, 6.5–8, and 8.5–9 by using buffering solutions of 2 mM MES, 3.6 mM MOPS, and 2 mM Tris, respectively, by the addition of 1 M NaOH or 1 M HCl.

3.2.4. Effect of major cations and anions on iAs(V) toxicity

The individual effects of the major cations (Ca^{2+}, Mg^{2+}, and K^{+}) and anions ($HPO_4^{2-}/H_2PO_4^{-}$, SO_4^{2-}, NO_3^{-}, and HCO_3^{-}) on iAs(V) toxicity were investigated at pH

7 in 3.6 mM MOPS buffer. The toxicity assays for iAs(V) included seven experimental sets: PO_4-set, SO_4-set, NO_3-set, HCO_3-set, Ca-set, Mg-set, and K-set. Each set consisted of a series of solutions with five different concentrations of major cations (0, 0.25, 1.3, 5, and 25 mM) and four different concentrations of major anions (i.e., 0, 0.25, 1.3, and 5 mM). Each test was conducted by the Extended (9 dilution) Test Method [32] with some modifications, to maintain the same concentration of major cations and anions in the tested solutions during the serial dilution procedure. The concentrations of iAs(V) in each test medium (i.e., in direct contact with *A. fischeri*) was in the range from 0.02 to 6.3 mM, except for the 25 mM PO_4-set, in which the range was from 0.1 to 25 mM. Analysis of variance (ANOVA) was performed by using Microsoft Excel 2010 Analysis ToolPak to evaluate whether the competition from the major cations and anions significantly influenced iAs(V) toxicity.

3.2.5. Derivation of iAs(V) toxicity prediction model parameters

The parameters of the toxicity prediction model for iAs(V) were derived from iAs(V) toxicity data obtained at pH 5 and 9 and the reconstruction of the original BLM approach. A detailed mathematical description of the developed model is shown in section 3.3.4. To derive the model parameters (K_{XHAsO4}, $K_{XH2AsO4}$, K_{XHPO4}, K_{XH2PO4}, and $f_{mix}^{50\%}$), iAs(V) toxicity tests were conducted with different phosphate concentrations (0, 0.25, 1.3, 5, and 25 mM) at pH 5 (2 mM MES buffer) and pH 9 (2 mM Tris buffer). At the respective phosphate concentrations, the calculated

$H_2PO_4^-$ activities were 0, 0.14, 0.68, 2.71, and 13.6 mM and the HPO_4^{2-} activities were 0, 0.03, 0.16, 0.65, and 3.1 mM.

3.2.6. Chemical analysis

The concentrations of major cations and iAs(V) were determined by using inductively coupled plasma atomic emission spectrometry (ICAP 7400 DUO, Thermo Scientific, Waltham, MA). The concentrations of the major anions were determined by using ion chromatography (DX500, Dionex, Sunnyvale, CA). In order to confirm whether a complex was formed between iAs(V) and the major cations (e.g., calcium arsenate), high performance liquid chromatography (HPLC) linked to inductively coupled plasma mass spectrometry (ICP-MS, Agilent 7700s, Agilent Technologies, Japan) was used. The separation of iAs(V) was achieved by using a Hamilton PRP X-100 anion exchange column with the eluent consisting of 2 mM NaH_2PO_4 and 0.2 mM EDTA (pH 6) [34]. Visual MINTEQ 3.1 [35] was used to calculate the activities of iAs(V) ($H_2AsO_4^-$ and $HAsO_4^{2-}$) and the major cations/anions in the tested solution. Temperature, pH, ion concentrations, and the partial pressure of CO_2 (i.e., P_{CO2} = 0.00038 atm) were used as the input data. Because each sample used in this study included 2% NaCl to control the osmotic pressure to *A. fischeri*, all speciation calculations included the corresponding Na^+ and Cl^- concentrations of 0.342 M.

3.3. Results and discussion

3.3.1. pH dependency of iAs(V) toxicity

The data in Figure 3.1 clearly show that pH increase results in enhanced toxicity of iAs(V).

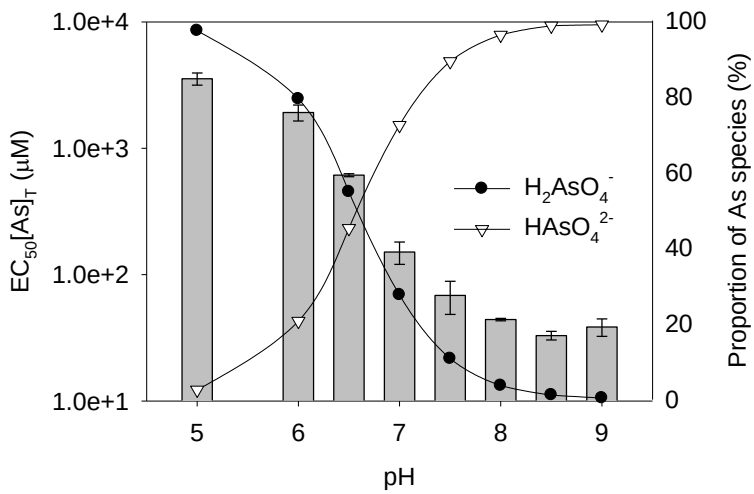

Figure 3.1. The measured EC50 values expressed as total iAs(V) concentration ($EC_{50}[As]_T$) (left y-axis; log scale) and the proportion of As species in solution (right y-axis) as a function of pH. Vertical bars represent the $EC_{50}[As]_T$. The error bars indicate the standard deviations (n = 3). The proportion of As species was computed by using Visual MINTEQ 3.1.

The $EC_{50}[As]_T$ value (the EC50 expressed as total dissolved concentration of iAs(V)) decreased from 3554 ± 393 μM to 39 ± 6 μM as the pH increased from 5 to 9. Taken the possible forms of iAs(V) depending on pK_a values into consideration (pK_{a1} = 2.26, pK_{a2} = 6.76, and pK_{a3} = 11.29), $H_2AsO_4^-$ form mainly existed at pH 5 and, as pH increased deprotonation proceeded and essentially all were present as $HAsO_4^{2-}$

form at pH 9. Fulladosa et al. [36] observed that the pH itself did not affect the calculated EC50 values of the standard chemical phenol, which showed that no toxicity resulted from the changes in the experimental pH (5 to 9).

For iAs(V) to express toxicity, it should be introduced into the cell interior, and inorganic phosphate (Pi) transporters, which is a cell membrane-embedded system, are known to be involved [11,37-39]. Indeed, the type II (NaPi-IIa, NaPi-IIb, and NaPi-IIc) and type III (PiT1 and PiT2) families of sodium-dependent phosphate cotransporters are reported, and they exhibit preference for phosphate forms: Type II family shows a greater specificity to monohydrogen phosphate (HPO_4^{2-}) and type III family has a preference for dihydrogen phosphate ($H_2PO_4^-$) [40]. For this reason, iAs(V) toxicity differs depending on pH although it has the same atomic valence of +5 (iAs(V)). Consequently, it is essential to develop a BLM that can reflect pH-dependency of iAs(V). Our results showed that such difference varies up to 91 times between pH 5 and 9 (Figure 3.1).

3.3.2. Effect of cations on iAs(V) toxicity

When the activities of Ca^{2+}, Mg^{2+}, and K^+ increased, no significant differences in the EC50 values expressed as $HAsO_4^{2-}$ activities (i.e., $EC_{50}\{HAsO_4^{2-}\}$) were shown by ANOVA (i.e., $p > 0.1$ in all cases) (Figure 3.2). Although the Ca^{2+} activity increased from 0 to 5.84 mM, the $EC_{50}\{HAsO_4^{2-}\}$ values varied from 31.2 to 47.0 μM (mean = 38.7 μM) with no statistically significant difference (Figure 3.2a). Mg^{2+} also showed the same tendency as Ca^{2+}, and K^+ also did not affect the iAs(V) toxicity even though it had a charge of +1 (Figure 3.2b-c).

We previously found [21] that Ca^{2+} and Mg^{2+} alleviated the toxicity of Cd^{2+} and Pb^{2+} to *A. fischeri*, due to the competitive effect among the cationic heavy metals for available BL sites. In contrast, iAs(V) is present as an anionic form in water and thus no competition was observed. Actually, the complexation between cations and iAs(V) was not observed by HPLC-ICP-MS analysis in this study (data not shown).

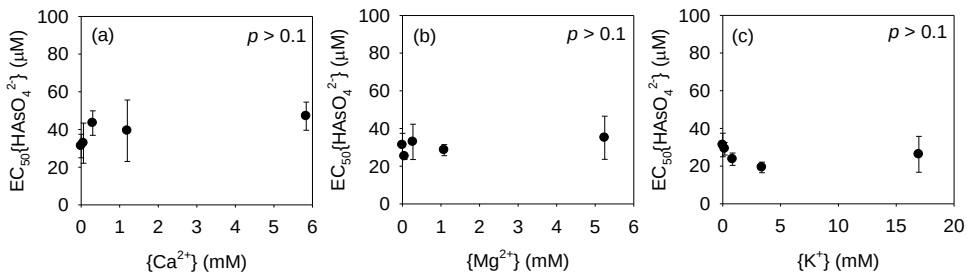

Figure 3.2. The effects of increased activities of major cations on $EC_{50}\{HAsO_4^{2-}\}$ obtained from the toxicity data conducted at pH 7: (a) Ca^{2+} set, (b) Mg^{2+} set, and (c) K^+ set. The error bars indicate the standard deviations (n = 3). No statistical significance between any sets was determined by analysis of variance (ANOVA).

3.3.3. Effect of anions on iAs(V) toxicity

Since iAs(V) is present as an anionic form in water, it is reasonable to assume that other anions such as phosphate (HPO_4^{2-} and $H_2PO_4^-$), sulfate (SO_4^{2-}), nitrate (NO_3^-), and bicarbonate (HCO_3^-), if present simultaneously, can compete with iAs(V) and thus influence on the toxicity of iAs(V). The results show that $EC_{50}\{HAsO_4^{2-}\}$ values significantly increased (ANOVA result: $p < 0.05$) from 31 ± 6 μM to 859 ± 128 μM as HPO_4^{2-} activity increased from 0 to 0.44 mM, yielding a strong linear correlation (Figure 3.3a). In contrast, the other anions did not seem to exhibit

competitive effect on active binding sites of *A. fischeri* because the simultaneous presence of SO_4^{2-}, NO_3^-, and HCO_3^- with $HAsO_4^{2-}$ did not cause statistically significant changes in $EC_{50}\{HAsO_4^{2-}\}$ values (Figure 3.3b-d).

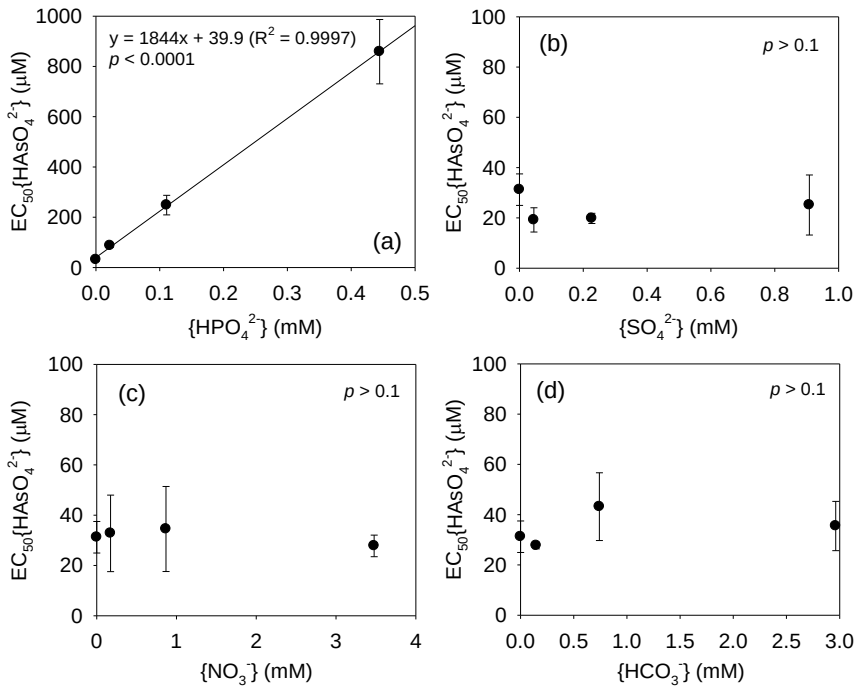

Figure 3.3. The effects of increased activities of major anions on $EC_{50}\{HAsO_4^{2-}\}$ obtained from toxicity data conducted at pH 7: (a) HPO_4^{2-} set, (b) SO_4^{2-} set, (c) NO_3^- set, and (d) HCO_3^- set. The error bars indicate the standard deviations (n = 3). The solid lines indicate the linear regression curves (i.e., ANOVA result: $p < 0.01$).

Our results suggest that not only the valence but also the chemical structure may play a key role in competition for active binding sites. The similarity in chemical structure between $HAsO_4^{2-}$ or $H_2AsO_4^-$ and HPO_4^{2-} or $H_2PO_4^-$ is well known, and this structural similarity is often used to extract As from soil with phosphate [42,43].

3.3.4. Development of extended BLM for prediction of iAs(V) toxicity

As previously noted, the existing BLM was modified to reflect changes in the iAs(V) toxicity by pH and phosphate concentration (or activity). One of the main assumptions of the BLM for cationic metals such as Cd, Cu, Ni, Pb, and Zn [21,24,26,27] is that positively charged free metal ions bind to the negatively charged BL sites on the cell membrane surface, and it has been revised to have a positively charged ABS that can also be attached to (oxy)anions. As discussed in section 3.3.1, $HAsO_4^{2-}$ appears more toxic to *A. fischeri* than $H_2AsO_4^-$. Considering the nature of BLM concept, it is reasonably understood that multivalent positive or negative ions are more toxic than monovalent ions. In general, the greater the affinity of metals for binding to the BL sites of the organisms (log *K* value) of a particular metal, the toxicity will be more severe [44,45]. If positively charged active binding sites (ABS) (i.e., counterparts of the BL sites in the existing BLM) are present in the cell membrane of *A. fischeri*, the stronger negative charge of $HAsO_4^{2-}$ enables stronger and increased binding to ABS than $H_2AsO_4^-$, thereby resulting in greater toxicity. Also, as discussed in section 3.3.3, phosphate exhibited competitive effect to iAs(V). Although the competition between iAs(V) and phosphates seems to occur in the cell cytoplasm after the introduction of iAs(V) into cell interior through membrane-embedded phosphate transporters, not to occur in the cell membrane of *A. fischeri* [11], the revised assumption that the ABS are presented on the cell membrane still provides a good explanation for the decrease in iAs(V) toxicity as the phosphate activity increased. As a simplified approximation to predict iAs(V) toxicity with

consideration of pH and phosphate effects, the reconstructed BLM was presented in Eq. 3.3 to 3.12, as described below.

Phosphate, as well as iAs(V), can react with positively charged ABS on the cell membrane surface of *A. fischeri*. This reaction can be expressed as shown in Eq. 3.3:

$$K_{XA} = \frac{[XA^{(n-1)-}]}{[X^{+}]\{A^{n-}\}} \tag{3.3}$$

where $[XA^{(n-1)-}]$ is the concentration of ABS-iAs(V) or the ABS-phosphate complex (mol/L), $[X^{+}]$ is the concentration of unoccupied ABS (mol/L), $\{A^{n-}\}$ is the activity of iAs(V) or phosphate (mol/L) in the bulk solution, and K_{XA} is the conditional binding constant for iAs(V) or phosphate bound to ABS (L/mol).

The concentration of total ABS ($[TX]$) can be expressed by Eq. 3.4, and the substitution of Eq. 3.4 with Eq. 3.3 yielded Eq. 3.5.

$$[TX] = [X^{+}] + [X - H_2AsO_4] + [X - HAsO_4^{-}] + [X - H_2PO_4] + [X - HPO_4^{-}] \tag{3.4}$$

$$[TX] = [X^{+}](1 + K_{XH2AsO4}\{H_2AsO_4^{-}\} + K_{XHAsO4}\{HAsO_4^{2-}\} + K_{XH2PO4}\{H_2PO_4^{-}\} + K_{XHPO4}\{HPO_4^{2-}\}) \tag{3.5}$$

The fraction of ABS occupied by both $H_2AsO_4^-$ and $HAsO_4^{2-}$ (f_{mix}) (Eq. 3.6) was proportional to the toxicity of *A. fischeri*, followed by the main hypotheses of the

original BLM for cationic metals [23,24]. The EC_{50} values can be described in Eq. 3.7.

$$f_{mix} = \frac{[X-H_2AsO_4]+[X-HAsO_4^-]}{[TX]} = \frac{K_{XH2AsO4}\{H_2AsO_4^-\}+K_{XHAsO4}\{HAsO_4^{2-}\}}{1+K_{XH2AsO4}\{H_2AsO_4^-\}+K_{XHAsO4}\{HAsO_4^{2-}\}+K_{XH2PO4}\{H_2PO_4^-\}+K_{XHPO4}\{HPO_4^{2-}\}} \quad (3.6)$$

$$EC_{50}\{HAsO_4^{2-}\} = \frac{f_{mix}^{50\%}(1+K_{XH2PO4}\{H_2PO_4^-\}+K_{XHPO4}\{HPO_4^{2-}\})}{(1-f_{mix}^{50\%})(\frac{K_{XH2AsO4}}{K_{As}}\{H^+\}+K_{XHAsO4})} \quad (3.7)$$

where $EC_{50}\{HAsO4^{2-}\}$ is the $HAsO_4^{2-}$ activity that results in 50% toxicity to *A. fischeri*, K_{As} is the acid dissociation constant of iAs(V) (pK_{As} = 6.76), and $f_{mix}^{50\%}$ is the *ABS* required to be occupied by iAs(V) (both $H_2AsO_4^-$ and $HAsO_4^{2-}$) to induce 50% toxicity.

At pH 5, Eq. 3.6 can be transformed into Eq. 3.8 and Eq. 3.9, as the activities of $H_2AsO_4^-$ and $H_2PO_4^-$ were much higher than those of $HAsO_4^{2-}$ and HPO_4^{2-}, respectively, because $K_{HAsO4}\{HAsO_4^{2-}\}$ and $K_{HPO4}\{HPO_4^{2-}\}$ are negligible at pH 5. Similarly, Eq. 3.6 can be converted into Eq. 3.10 and Eq. 3.11 at pH 9, because $K_{H2AsO4}\{H_2AsO_4^-\}$ and $K_{H2PO4}\{H_2PO_4^-\}$ are negligible at pH 9.

$$f_{XH2AsO4} = \frac{[X-H_2AsO_4]}{[TX]} = \frac{K_{XH2AsO4}\{H_2AsO_4^-\}}{1+K_{XH2AsO4}\{H_2AsO_4^-\}+K_{XH2PO4}\{H_2PO_4^-\}} \quad (3.8)$$

$$EC_{50}\{H_2AsO_4^-\} = (\frac{f_{XH2AsO4}^{50\%}}{1-f_{XH2AsO4}^{50\%}})\frac{(1+K_{XH2PO4}\{H_2PO_4^-\})}{K_{XH2AsO4}} \quad (3.9)$$

$$f_{XHAsO4} = \frac{[X - HAsO_4]}{[TX]} = \frac{K_{XHAsO4}\{HAsO_4^{2-}\}}{1 + K_{XHAsO4}\{HAsO_4^{2-}\} + K_{XHPO4}\{HPO_4^{2-}\}} \quad (3.10)$$

$$EC_{50}\{HAsO_4^{2-}\} = \left(\frac{f_{XHAsO4}^{50\%}}{1 - f_{XHAsO4}^{50\%}}\right)\frac{(1 + K_{XHPO4}\{HPO_4^{2-}\})}{K_{XHAsO4}} \quad (3.11)$$

Where $f_{XH2AsO4}^{50\%}$ and $f_{XHAsO4}^{50\%}$ are the *ABS* required to be occupied by $H_2AsO_4^-$ and $HAsO_4^{2-}$, respectively, to induce 50% toxicity.

As illustrated in Eq. 3.9 and Eq. 3.11, the linear relationship between the EC50 value at a given pH and the phosphate activity should be observed if a competitive effect of ABS and iAs(V) occurs. Hence, the conditional binding constants of phosphate (K_{XH2PO4} and K_{XHPO4}) were derived from the slope and the intercept of the linear relationships (Figure 3.4a–b), as shown by De Schamphelaere and Janssen [24]. The determined values were 3.424 for logK_{XH2PO4} and 4.588 for logK_{XHPO4}, respectively.

$K_{XH2AsO4}$ and K_{XHAsO4} were determined through the optimization of the linear relationship between the logit transformed toxic effect and the fraction of *ABS* occupied by $H_2AsO_4^-$ at pH 5 and $HAsO_4^{2-}$ at pH 9, respectively [24,41]. The best approximation results between the logit of the measured toxic effect and the calculated the fraction of the occupied ABS were determined to be 3.067 for log$K_{XH2AsO4}$ and 4.802 for logK_{XHAsO4}, respectively (Figure 3.4c–d). The values of $f_{XH2AsO4}^{50\%}$ and $f_{XHAsO4}^{50\%}$ were calculated to be 0.6979 and 0.5556, respectively.

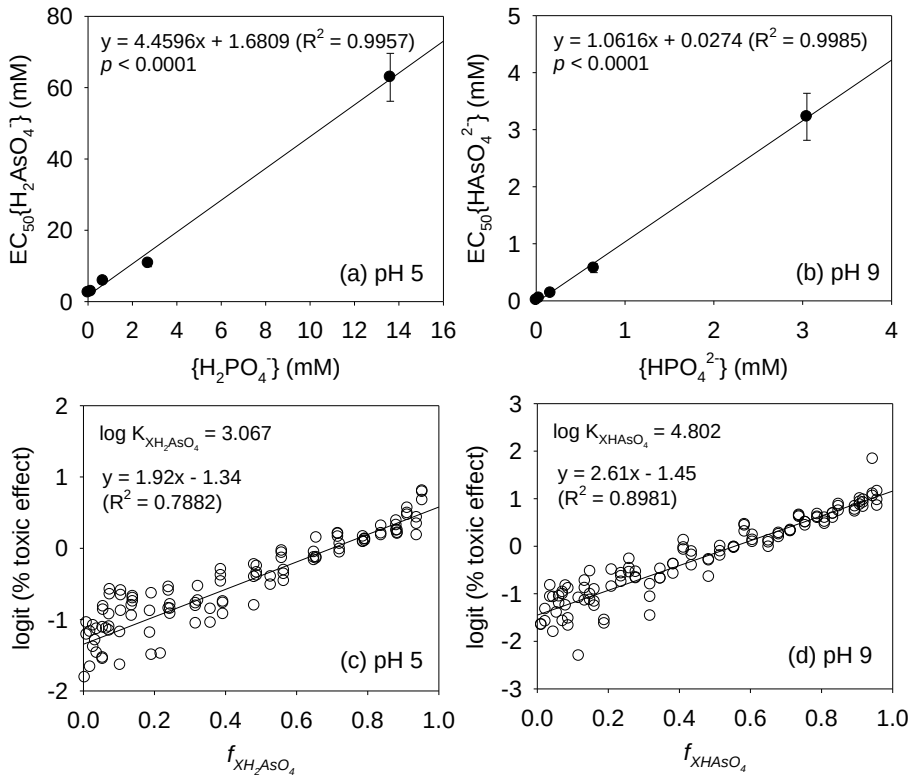

Figure 3.4. The derivation of BLM parameters at different pH values: Linear relationships between (a) $EC_{50}\{H_2AsO_4^-\}$ and $H_2PO_4^-$ activity at pH 5 and (b) $EC_{50}\{HAsO_4^{2-}\}$ and HPO_4^{2-} activity at pH 9. In accordance with the method of De Schamphelaere and Janssen [24], the conditional binding constants between phosphate and BL sites were determined as 3.424 for K_{XH2PO4} and 4.588 for K_{XHPO4} by using the slopes and intercepts of the linear relationships. The best approximation results between the logit of the measured toxic effect and the calculated fraction of BL sites occupied by $H_2AsO_4^-$ or $HAsO_4^{2-}$ are shown: (c) for $H_2AsO_4^-$ at pH 5, log $K_{XH2AsO4}$ was 3.067, and (d) for $HAsO_4^{2-}$ at pH 9, log K_{XHAsO4} was 4.802.

An et al. [21] developed BLMs able to predict toxicity of Cd and Pb to *A. fischeri*. A competitive effect of cations was observed, and the derived parameters were 5.02 for $\log K_{CdBL}$, 0.435 for $f_{CdBL}^{50\%}$, 6.67 for $\log K_{PbBL}$, and 0.547 for $f_{PbBL}^{50\%}$. In this case,

the $\log K_{CaBL}$ value, which indicates the magnitude of the competitive effect of Ca^{2+}, was 2.84 for Cd or 2.30 for Pb [21]. Through the use of these conditional binding constants, the magnitude of the toxicity and competitive effect can be compared. The ability of phosphate to alleviate iAs(V) toxicity is much greater than that of Ca^{2+} to alleviate Cd or Pb toxicity, which is presumably a result of the structural similarity between phosphate and iAs(V).

Finally, the parameter $f_{mix}^{50\%}$ was derived through the substitution of the experimentally determined toxic effect (R) and the corresponding f_{mix} (Eq. 3.5) in Eq. 3.12.

$$R = \frac{100}{1 + (\frac{f_{mix}}{f_{mix}^{50\%}})^{\beta}} \tag{3.12}$$

Where R is the toxic effect (i.e., percentage bioluminescence inhibition) of iAs(V) to *A. fischeri*, and β is the fitting parameter that determines the shape of the dose-response curve.

The derived $f_{mix}^{50\%}$ was 0.6161 as shown in Figure 3.5. This value was in good agreement with the average value (0.6267) of $f_{XH2AsO4}^{50\%}$ and $f_{XHAsO4}^{50\%}$ calculated by other means. From Eq. 3.7, all determined parameters (i.e., K_{XHAsO4}, $K_{XH2AsO4}$, K_{XHPO4}, K_{XH2PO4}, $f_{mix}^{50\%}$), $EC_{50}\{HAsO_4^{2-}\}$ can be calculated from the activities of competing phosphates and pH. Thus, Eq. 3.7 can be transformed for the calculation of

$EC_{50}\{H_2AsO_4^-\}$, as well as $EC_{50}[As]_T$.

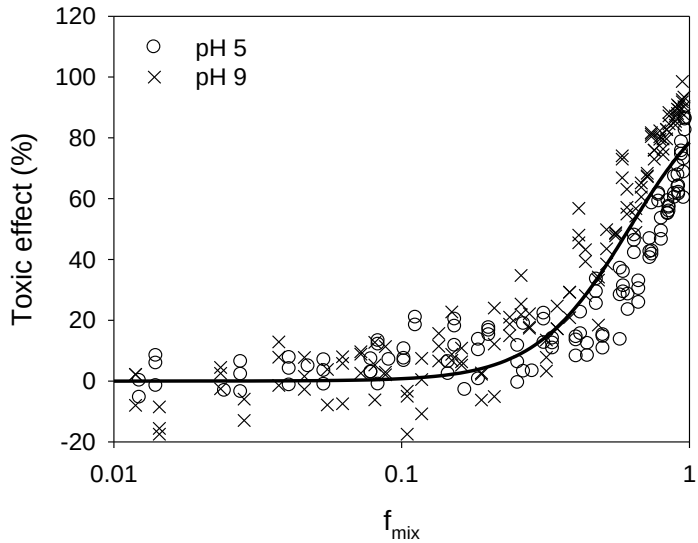

Figure 3.5. The dose-response relationships between the toxic effects to *A. fischeri* measured at pH 5 (○) and 9 (×) at different phosphate activities (i.e., $\{H_2PO_4^-\}$ = 0, 0.14, 0.68, 2.71, and 13.6 mM at pH 5, $\{HPO_4^{2-}\}$ = 0, 0.03, 0.16, 0.65, and 3.05 mM at pH 9) and f_{mix} value calculated from Eq. 3.6. The solid lines indicate the logistic curve fitted to all data.

3.3.5. Validation of extended BLM

The model to predict iAs(V) toxicity was developed by using data from toxicity tests performed at pH 5 and 9 in the presence of various phosphate concentrations (Figure 3.4 and Figure 3.5). In order to validate the developed model, the measured toxic effects, which were obtained at different pH values from 5.5 to 8.5 (section 3.3.1) and different phosphate concentrations from 0 to 5 mM at pH 7 (section 3.3.3), were compared with the predicted values (Figure 3.6). Model-predicted $EC_{50}\{HAsO_4^{2-}\}$ in a range of 2.29E-05 to 2.44E-03 M and experimentally

determined $EC_{50}\{HAsO_4^{2-}\}$ in a range of 8.64E-06 to 5.07E-03 M had a strong linear relationship within an order of magnitude (Figure 3.6). It demonstrated that site-specific iAs(V) toxicity was effectively predicted by using the developed iAs(V) toxicity prediction model with the water chemistry.

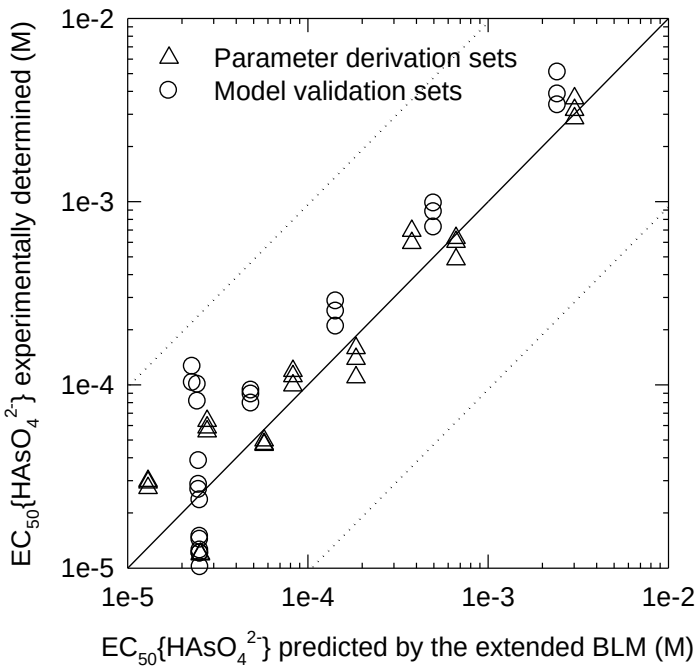

Figure 3.6. The linear relationship between the experimentally determined $EC_{50}\{HAsO_4^{2-}\}$ at different pH values and the predicted EC_{50} from the developed models. The solid line represents a 1:1 match between the measured and predicted EC_{50} values. The BLM parameters were derived from toxicity data with varying phosphate activities at pH 5 and 9 (parameter derivation sets: △) and the predictive power of the model can be effectively evaluated by using toxicity data conducted at pH 7 (model validation sets: ○).

3.4. Summary

BLM was extended to predict the toxicity of iAs(V) to the luminescent bacteria, *A. fischeri*. As the pH increased from 5 to 9, the $HAsO_4^{2-}$ form predominated more than $H_2AsO_4^-$, and the $EC_{50}[As]_T$ (50% effective iAs(V) concentration) decreased drastically from 3554 ± 393 to 39 ± 6 μM; thus, the $HAsO_4^{2-}$ form was more toxic to *A. fischeri* than $H_2AsO_4^-$. As the HPO_4^{2-} activity increased from 0 to 0.44 mM, the $EC_{50}\{HAsO_4^{2-}\}$ values (50% effective $HAsO_4^{2-}$ activity) increased from 31 ± 6 to 859 ± 128 μM, indicating that the toxicity of iAs(V) decreased, owing to the competition caused by the structural similarity between iAs(V) and phosphate ions. However, activities of Ca^{2+}, Mg^{2+}, K^+, SO_4^{2-}, NO_3^-, and HCO_3^- did not significantly affect the $EC_{50}\{HAsO_4^{2-}\}$ values. The BLM was reconstructed to take into account the effects of pH and phosphate, and the conditional binding constants for $H_2PO_4^-$, HPO_4^{2-}, $H_2AsO_4^-$, and $HAsO_4^{2-}$ to the active binding sites of *A. fischeri* were obtained; 3.424 for $\log K_{XH2PO4}$, 4.588 for $\log K_{XHPO4}$, 3.067 for $\log K_{XH2AsO4}$, and 4.802 for $\log K_{XHAsO4}$. The fraction of active binding sites occupied by iAs(V) to induce 50% toxicity ($f_{mix}^{50\%}$) was found to be 0.616.

References

[1] B.K. Mandal, K.T. Suzuki, Arsenic round the world: a review, Talanta 58 (2002) 201-235.

[2] P.L. Smedley, D.G. Kinniburgh, A review of the source, behaviour and distribution of arsenic in natural waters, Appl. Geochem. 17 (2002) 517-568.

[3] D. Das, G. Samanta, B.K. Mandal, T.R. Chowdhury, C.R. Chanda, P.P. Chowdhury, G.K. Basu, D. Chakraborti, Arsenic in groundwater in six districts of West Bengal, India, Environ. Geochem. Health 18 (1996) 5-15.

[4] J. Susaya, K.-H. Kim, M.C. Jung, The impact of mining activities in alteration of As levels in the surrounding ecosystems: An encompassing risk assessment and evaluation of remediation strategies, J. Hazard. Mater. 182 (2010) 427-438.

[5] C.C. Tanner, J.S. Clayton, Persistence of arsenic 24 years after sodium arsenite herbicide application to Lake Rotoroa, Hamilton, New Zealand, New Zeal. J. Mar. Fresh. 24 (1990) 173-178.

[6] J.A. Hingston, C.D. Collins, R.J. Murphy, J.N. Lester, Leaching of chromated copper arsenate wood preservatives: a review, Environ. Pollut. 111 (2001) 53-66.

[7] V.K. Sharma, M. Sohn, Aquatic arsenic: Toxicity, speciation, transformations, and remediation, Environ. Int. 35 (2009) 743-759.

[8] Q. Xie, R. Kerrich, E. Irving, K. Liber, F. Abou-Shakra, Determination of five arsenic species in aqueous samples by HPLC coupled with a hexapole

collision cell ICP-MS, J. Anal. At. Spectrom. 17 (2002) 1037-1041.

[9] P.R. Paquin, J.W. Gorsuch, S. Apte, G.E. Batley, K.C. Bowles, P.G.C. Campbell, C.G.. Delos, D.M. Di Toro, R.L. Dwyer, F. Galvez, R.W. Gensemer, G.G. Goss, C. Hogstrand, C.R. Janssen, J.C. McGeer, R.B. Naddy, R.C. Playle, R.C. Santore, U. Schneider, W.A. Stubblefield, C.M. Wood, K.B. Wu, The biotic ligand model: A historical overview, Comp. Biochem. Physiol. 133C (2002) 3-35.

[10] J.C. McGeer, R.C. Playle, C.M. Wood, F. Galvez, A physiologically based biotic ligand model for predicting the acute toxicity of waterborne silver to rainbow trout in freshwaters, Environ. Sci. Technol. 34 (2000) 4199-4207.

[11] D.A. Rubinos, V. Calvo, L. Iglesias, M.T. Barral, Acute toxicity of arsenic to *Aliivibrio fischeri* (Microtox® bioassay) as influenced by potential competitive-protective agents, Environ. Sci. Pollut. Res. 21 (2014) 8631-8644.

[12] W.J.G.M. Peijnenburg, T. Jager, Monitoring approaches to assess bioaccessibility and bioavailability of metals: matrix issues, Ecotoxicol. Environ. Saf. 56 (2003) 63-77.

[13] A. Kungolos, P. Samaras, V. Tsiridis, M. Petala, G. Sakellaropoulos, Bioavailability and toxicity of heavy metals in the presence of natural organic matter, J. Environ. Sci. Health, Part A 41 (2006) 1509-1517.

[14] P.L. Brown, S.J. Markich, Evaluation of the free ion activity model of metal-organism interaction: Extension of the conceptual model, Aquat. Toxicol. 51 (2000) 177-194.

[15] R.J. Erickson, D.A. Benoit, V.R. Mattson, H.P. Nelson Jr, E.N. Leonard,

The effects of water chemistry on the toxicity of copper to *fathead minnows*, Environ. Toxicol. Chem. 15 (1996) 181-193.

[16] K. Lock, C.R. Janssen, Influence of aging on metal availability in soils, Rev. Environ. Contam. Toxicol. 178 (2003) 1-21.

[17] R. Lanno, J. Wells, J. Conder, K. Bradham, N. Basta, The bioavailability of chemicals in soil for earthworms, Ecotoxicol. Environ. Saf. 57 (2004) 39-47.

[18] C.A.M. Van Gestel, J.E. Koolhaas, Water-extractability, free ion activity, and pH explain cadmium sorption and toxicity to *Folsomia candida* (collembola) in seven soil-pH combinations, Environ. Toxicol. Chem. 23 (2004) 1822-1833.

[19] D.T. Lamb, M. Kader, L. Wang, G. Choppala, M.M. Rahman, M. Megharaj, R. Naidu, Pore-water carbonate and phosphate as predictors of arsenate toxicity in soil, Environ. Sci. Technol. 50 (2016) 13062-13069.

[20] P. Wang, D. Zhou, T.B. Kinraide, X. Luo, L. Li, D. Li, H. Zhang, Cell membrane surface potential (Ψ_0) plays a dominant role in the phytotoxicity of copper and arsenate, Plant Physiol. 148 (2008) 2134-2143.

[21] J. An, S. Jeong, H.S. Moon, E.H. Jho, K. Nam, Predication of Cd and Pb toxicity to *Vibrio fischeri* using biotic ligand-based models in soil, J. Hazard. Mater. 203-204 (2012) 69-76.

[22] J. An, E.H. Jho, K. Nam, Effect of dissolved humic acid on the Pb bioavailability in soil solution and its consequence on ecological risk, J. Hazard. Mater. 286 (2015) 236-241.

[23] D.M. Di Toro, H.E. Allen, H.L. Bergman, J.S. Meyer, P.R. Paquin, R.C.

Santore, Biotic ligand model of the acute toxicity of metals. 1. Technical basis, Environ. Toxicol. Chem. 20 (2001) 2383-2396.

[24] K.A.C. De Schamphelaere, C.R. Janssen, A biotic ligand model predicting acute copper toxicity for *Daphnia magna*: The effects of calcium, magnesium, sodium, potassium, and pH, Environ. Sci. Technol. 36 (2002) 48-54.

[25] X.S. Luo, L.Z. Li, D.M. Zhou, Effect of cations on copper toxicity to wheat root: Implications for the biotic ligand model, Chemosphere 73 (2008) 401-406.

[26] S. Thakali, H.E. Allen, D.M. Di Toro, A. A. Ponizovsky, C. P. Rodney, F. J. Zhao, S. P. McGrath, A Terrestrial Biotic Ligand Model. 1. Development and application to Cu and Ni toxicities to barley root elongation in soils, Environ. Sci. Technol. 40 (2006) 7085-7093.

[27] X. Wang, B. Li, Y. Ma, L. Hua, Development of a biotic ligand model for acute zinc toxicity to barley root elongation, Ecotoxicol. Environ. Saf. 73 (2010) 1272-1278.

[28] N.-X. Wang, Y. Li, X.-H. Deng, A.-J. Miao, R. Ji, L.-Y. Yang, Toxicity and bioaccumulation kinetics of arsenate in two freshwater green algae under different phosphate regimes, Water research 47 (2013) 2497-2506.

[29] B.-C. Chen, W.-Y. Chen, C.-M. Liao, A biotic ligand model-based toxicodynamic approach to predict arsenic toxicity to tilapia gills in cultural ponds, Ecotoxicology 18 (2009) 377-383.

[30] J.-W. Tsai, W.-Y. Chen, Y.-R. Ju, C.-M. Liao, Bioavailability links mode of action can improve the long-term field risk assessment for tilapia exposed

to arsenic, Environ. Int. 35 (2009) 727-736.

[31] H. Urbanczyk, J.C. Ast, M.J. Higgins, J. Carson, P.V. Dunlap, Reclassification of *Vibrio fischeri*, *Vibrio logei*, *Vibrio salmonicida* and *Vibrio wodanis* as *Aliivibrio fischeri* gen. nov., comb. nov., *Aliivibrio logei* comb. nov., *Aliivibrio salmonicida* comb. nov. and *Aliivibrio wodanis* comb. nov., Int. J. Syst. Evol. Microbiol. (2007) 2823-2829.

[32] Microbics Corp., Microtox Manual, A Toxicity Testing Hand book, Microbics Corp., Carlsbad, CA, USA, 1992.

[33] L. Haanstra, P. Doelman, J.H. Oude Voshaar, The use of sigmoidal dose response curves in soil ecotoxicological research, Plant Soil 84 (1985) 293-297.

[34] J. An, K.-H. Kim, J.-A. Kim, H. Jung, H.-O. Yoon, J. Seo, A simplified analysis of dimethylarsinic acid by wavelength dispersive X-ray fluorescence spectrometry combined with a strong cation exchange disk, J. Hazard. Mat. 260 (2013) 24-31.

[35] Gustafsson, J.P., 2014, Visual MINTEQ, Ver 3.1, available from http://vminteq.lwr.kth.se/ (accessed December, 2016).

[36] E. Fulladosa, J.C. Murat, M. Martinez, I. Villaescusa, Effect of pH on arsenate and arsenite toxicity to luminescent bacteria (Vibrio fischeri), Arch. Environ. Contam. Toxicol. 46 (2004) 176-182.

[37] R. Villa-Bellosta, V. Sorribas, Role of rat sodium/phosphate cotranporters in the cell membrane transport of arsenate, Toxicol. Appl. Pharmacol. 232 (2008) 125-134.

[38] R. Villa-Bellosta, V. Sorribas, Arsenate transport by sodium/phosphate

cotransporter type IIb, Toxicol. Appl. Pharmacol. 247 (2010) 36-40.

[39] E.M. Muehe, J.F. Eisele, B. Daus, A. Kappler, K. Harter, C. Chaban, Are rice (*Oryza sativa* L.) phosphate transporters regulated similarly by phosphate and arsenate? A comprehensive study, Plant Mol. Biol. 85 (2014) 301-316.

[40] J. Marks, E.S. Debnam, R.J. Unwin, Phosphate homeostasis and the renal-gastrointestinal axis, Am. J. Physiol. Renal Physiol. 299 (2010) F285-F296.

[41] K. Lock, H. Van Eeckhout, K.A.C. De Schamphelaere, P. Criel, C.R. Janssen, Development of a biotic ligand model (BLM) predicting nickel toxicity to barley (*Hordeum vulgare*), Chemosphere 66 (2007) 1346-1352.

[42] J. Im, K. Yang, S. Moon, Y.-J. Kim, K. Nam, Role of phosphate and Fe-oxides on the acid-aided extraction efficiency and readsorption of As in field-aged soil, J. Hazard. Mater. 300 (2015) 161-166.

[43] J.Im, Y.-J. Kim, K. Yang, K. Nam, Applicability of soil washing with neutral phosphate for remediation of arsenic-contaminated soil at the former Janghang smelter site, J. Soil Groundw. Environ. 19(4) (2014) 45-51. (in Korean)

[44] M.M. Ardestani, N.M. van Straalen, C.A.M. van Gestel, The relationship between metal toxicity and biotic ligand binding affinities in aquatic and soil organisms: A review, Environ. Pollut. 195 (2014) 133-147.

[45] S. Niyogi, C.M. Wood, Biotic ligand model a flexible tool for developing site-specific water quality guidelines for metals, Environ. Sci. Technol. 38 (2004) 6177-6192.

CHAPTER 4

Use of the Extrapolated Biotic Ligand Model to Predict Arsenate Toxicity in Barley *Hordeum vulgare* Considering Cell Membrane Surface Electrical Potential

4.1. Introduction

Arsenic (As) accumulates in environmental media via both natural and anthropogenic sources, and can cause severe adverse effects not only to human health but also to ecosystems [1-3]. Because the total As concentration in the environmental media is not a good indicator of bioavailability or ecotoxicity, it is important to rationally assess ecotoxicity of As by using appropriate bioassays. The ecotoxicity of As varies greatly according to the environmental factors (e.g., phosphate concentration) in which the bioassay is performed [4,5] and to the sensitivity of the species tested [6]. The former can be considered using the biotic ligand model (BLM) that is a semi-mathematical and equilibrium model that predicts site-specific toxicity of cationic metals such as Cu, Ni, and Zn [7-9]. Recently, An et al. [10] developed a BLM for inorganic arsenate (iAs(V)), which is a dominant species in surface water and surface soil porewater. This BLM can effectively predict

the toxicity of iAs(V) to the bioluminescence *Aliivibrio fischeri* considering phosphate competition (toxicity alleviation) and As species alteration by pH. The latter can be considered using species sensitivity distribution (SSD), which is the cumulative distribution of toxicity of a single compound to a set of species that constitutes a community [11]. SSD can estimate the 5% hazardous concentration (HC5) that is defined as the total dissolved concentration of the contaminant that protects 95% of the species in the ecosystem.

To overcome site-specificity and species-specificity concurrently when assessing ecotoxicity and thereby deriving a safe concentration (e.g., HC5) in the ecosystem when combining BLM and SSD, the full species sensitivity distribution bioavailability normalization approach [12-15] can be used. With this approach, HC5 is estimated by an SSD obtained from the entire normalized (i.e., site-specific physicochemical properties that can affect toxicity of metals or metalloids reflected using BLM) ecotoxicity dataset. This approach assumes that some species may also share BLM parameters, i.e., conditional binding constants between free metal ions or major cations and active binding sites (i.e., biotic ligand) at the cell membrane surface of the organism [15]. Such an assumption has been proven by the evidence that BLMs for Cu, Ni, and Zn can be extrapolated across species [12-14,16].

To the best of our knowledge, the BLM for iAs(V) considers only the effect of phosphate competition on *A. fischeri*, as developed by our previous research [10], and not for individual species. Evidence supporting extrapolation with respect to the BLM for iAs(V) is still scarce. Therefore, in the present study, the feasibility of interspecies extrapolation was tested to extend the BLM for iAs(V) to a terrestrial

plant barley *Hordeum vulgare*, which is a sensitive species that can represent a terrestrial SSD. To confirm the predictability of BLM for iAs(V) after adjustment for the inherent sensitivity (IS) of *H. vulgare*, the predicted and measured 50% effective iAs(V) activity ($EC_{50}\{HAsO_4^{2-}\}$) was compared.

Meanwhile, the phenomenon that major cations alleviate metal toxicity can be explained in terms of not only BLM but also by the cell plasma membrane (PM) electrical potential (Ψ_0) concept [17-19]. The root cell PM surface, which is negatively charged, attracts cations in the bulk-phase medium. This indicates that the addition of major cations such as Ca^{2+} to the solution increases the Ψ_0, and decreases the cationic free metal ions moving to the cell PM surface by electrostatic attraction [17]. Conversely, iAs(V), which is normally present as $H_2AsO_4^-$ and $HAsO_4^{2-}$, can be accumulated on the PM surface. Wang et al. [18] found that a significant increase in iAs(V) toxicity to wheat (*Triticum aestivum*) as increasing Ca^{2+} activity in the bulk solution. This was attributed to the fact that the increase of Ca^{2+} activity from 0.2 to 2.5 mM in the solution increased Ψ_0 from -40 to -20 mV, resulting in a higher accumulation of $H_2AsO_4^-$ and $HAsO_4^{2-}$ on the root cell PM surface of *T. aestivum*. Such an increase in iAs(V) toxicity cannot be explained by the current BLM for iAs(V) [10].

The aim of the present study was to evaluate the feasibility of interspecies extrapolation of BLM for iAs(V), which was previously developed using *A. fischeri*, to a terrestrial plant *H. vulgare*, and to incorporate the Ψ_0 concept into the extrapolated BLM for iAs(V) to reflect the increased toxicity of iAs(V) by Ca^{2+}. It was expected that the acute BLM for iAs(V) developed for one bacteria would be

able to predict the iAs(V) toxicity to terrestrial plant species among various physicochemical properties by optimizing the IS.

4.2. Materials and methods

4.2.1. Ecotoxicity test with *H. vulgare*

The root growth inhibition test with barley *H. vulgare* was performed based on ISO guideline 11269-1 [20] with some modifications. Seeds were sterilized in a 5% NaOCl solution (Daejung, Korea) for 10 min, and rinsed three times with deionized (DI) water, with a resistance of 18.2 MΩ cm (Milli-Q, Millipore, Bedford, MA). Then, the seeds were germinated on filter paper moistened with DI water for 36 h at room temperature (25°C) in complete darkness. Each germinated seed was fixed in a polyethylene sheet floating on the surface of the medium. For each medium, a toxicity test was conducted, consisting of seven treatments (control + six different concentrations of iAs(V)). Each treatment was performed with six germinated seeds in a polyethylene beaker that was filled with 500 mL of test medium as a hydroponic culture. All test media were incubated during 5 d of exposure at 20°C with a light:dark cycle of 16:8 in a growth chamber (E15, Conviron, Canada). The toxicity of iAs(V), measured as relative root elongation (RRE) (Eq. 4.1), after exposure to a given concentration of iAs(V) was calculated [21] as follows.

$$\mathrm{RRE} = 100 \times \frac{L_{f,t} - L_{i,t}}{L_{f,c} - L_{i,c}} \quad (4.1)$$

Where RRE is the relative root elongation (%), $L_{f,t}$ is the average root length (mm) of each treatment after 5 d exposure, $L_{i,t}$ is the average root length (mm) of each treatment at initial time (t = 0), $L_{f,c}$ is the average root length (mm) of the control after 5 d exposure, and $L_{i,c}$ is the average root length (mm) of the control at initial time.

The changes in the RRE in response to changes in iAs(V) concentrations or activities were fitted to sigmoidal dose-response curve (Eq. 4.2) to calculate the 50% effective concentration (EC50) value.

$$y = y_0 + \frac{a}{1 + e^{-\frac{x - x_0}{b}}} \quad (4.2)$$

Where y is the observed RRE, x is the natural logarithm of an exposed iAs(V) concentration or activity, and, a, b, x_0, and y_0 are the fitting parameter that determines the shape of the dose-response curve.

A stock solution of iAs(V) (10 mM) was prepared by dissolving $Na_2HAsO_4 \cdot 7H_2O$ (98.0%–102%, Sigma-Aldrich) in DI water, and stored in the dark at 4°C prior to use. The concentrations of iAs(V) in each test medium (i.e., in direct contact with *H. vulgare*) were 0, 0.5, 2, 10, 50, 200, and 1000 μM. The pH of each test medium was adjusted to 7 ± 0.05 using 3.6 mM of 3-[N-morpholino]

propanesulfonic acid (MOPS, > 99.5%, Sigma), with the addition of 1 M NaOH or 1 M HCl. Background concentrations of major cations and anions in each test medium were Ca^{2+} = 0.2 mM, Mg^{2+} = 0.05 mM, K^{+} = 0.2 mM, Na^{+} = 1 mM, PO_4^{3-} = 0.05 mM, SO_4^{2-} = 0.05 mM, CO_3^{2-} = 0.2 mM, and NO_3^{-} = 0.2 mM. The individual effect of Ca^{2+} on iAs(V) toxicity to *H. vulgare* was assessed at pH 7 in 3.6 mM MOPS buffer. Each set consisted of a series of solutions with five different concentrations of Ca^{2+} (0.2, 1, 5, 10, and 20 mM) in the presence of a low phosphate concentration (i.e., background level = 0.05 mM) and a high phosphate concentration (5 mM).

The concentrations of major cations and iAs(V) were determined using inductively coupled plasma atomic emission spectrometry (ICAP 7400 DUO, Thermo Scientific, Waltham, MA). The concentrations of the major anions were determined using ion chromatography (DX500, Dionex, Sunnyvale, CA). The concentrations of dissolved organic carbon were determined using a total organic carbon analyzer (V-CPH, Shimadzu, Japan). Preliminary tests showed that the measured concentrations did not differ significantly from their nominal values within 5% variability.

Visual MINTEQ 3.1 [22] was used to calculate the activities of iAs(V) ($H_2AsO_4^{-}$ and $HAsO_4^{2-}$) and the major cations/anions in the tested solution. Temperature, pH, ion concentrations, and the partial pressure of CO_2 (P_{CO2} = 0.00038 atm) were used as the input data.

Analysis of variance (ANOVA) was performed using Microsoft Excel 2010 Analysis ToolPak to evaluate whether the Ca^{2+} significantly ($p < 0.05$) affected

iAs(V) toxicity.

4.2.2. Calculation of the electrical potential of root cell plasma membrane surface

To calculate Ψ_0 (the electrical potential of the root cell PM surface), and the corresponding ion activities at the PM surface, the Gouy-Chapman-Stern (GCS) model [19] was employed. The GCS model consists of two parts as follows: (i) electrostatic theory (Gouy-Chapman theory), and (ii) interaction between ions and the PM surface (Stern portion). The calculation process is briefly shown below.

First, the actual PM surface charge density (σ, unit: C/m^2) was described using Eq. 4.3.

$$\sigma^2 = 2\varepsilon_r\varepsilon_0 RT \sum_i [I^z]_b (\exp[\frac{-Z_i F \Psi_0}{RT}] - 1) \quad (4.3)$$

Where $2\varepsilon_r\varepsilon_0$RT = 0.00345 when concentrations are expressed in mol/L at 25°C. ε_r is the dielectric constant for water, ε_0 is the permittivity of a vacuum, and F, R, and T are the Faraday constant, gas constant, and absolute temperature, respectively. $[I^Z]_b$ is the free ion concentration in the bulk solution. Z_i is the charge on the i*th* ion.

Second, if the PM surface binding sites consisting of negatively charged sites (R^-) and neutral sites (P^0) are occupied by ions (I^Z), then the PM surface species and their equilibrium reactions can be presented as Eq. 4.4 and Eq. 4.5.

$$K_{RI} = \frac{[RI^{Z-1}]}{[R^-][I^Z]_0} \quad (4.4)$$

$$K_{PI} = \frac{[PI^Z]}{[R^0][I^Z]_0} \quad (4.5)$$

Where $[R^-]$, $[P^0]$, $[RI^{Z-1}]$, and $[PI^Z]$ denote PM surface densities expressed in mol/m^2. $[I^Z]_0$ denotes the concentration of the unbound ion I^Z at the PM surface.

Finally, the σ in the Graham equation (Eq. 4.3) can also be expressed as Eq. 4.6.

$$\sigma = \{-[R^-] + \sum_i (Z_i - 1)[RI^{Z-1}] + \sum_i (Z_i)[PI^Z]\}F \quad (4.6)$$

To calculate the values of $[I^Z]_0$, the Boltzmann equation (Eq. 4.7) can be used.

$$[I^z]_0 = [I^z]_b \exp(\frac{-Z_i F \Psi_0}{RT}) \quad (4.7)$$

To determine Ψ_0, trial values were assigned to Ψ_0 in Eq. 4.3 to 4.7 until the values for σ computed in Eq. 4.3 to 4.6 converged. The equilibrium constants and total surface densities of binding sites R and P in Eq. 4.4 and 4.5 were previously determined, and available from the study of Kopittke et al. [23].

4.2.3. Interspecies extrapolation of BLM

The BLM for predicting iAs(V) toxicity to *A. fischeri* previously reported [10] is presented in Eq. 4.8.

$$EC_{50}\{\mathrm{HAsO_4}^{2-}\} = \frac{f_{mix}^{50\%}\left[1+K_{XH2PO4}\{H_2PO_4{}^-\}+K_{XHPO4}\{HPO_4{}^{2-}\}\right]}{(1-f_{mix}^{50\%})\left[\frac{K_{XH2AsO4}}{K_{As}}\{H^+\}+K_{XHAsO4}\right]} \quad (4.8)$$

Where K_{XA} is the conditional binding constant for iAs(V) or phosphate bound to the active binding site (ABS) (L/mol), $\{A^{n-}\}$ is the activity of iAs(V) or phosphate (mol/L) in the bulk solution, K_{As} is the acid dissociation constant of iAs(V) (pK_{As} = 6.76), and $f_{mix}^{50\%}$ is the *ABS* required to be occupied by iAs(V) (both $H_2AsO_4^-$ and $HAsO_4^{2-}$) to induce 50% toxicity [10]. The BLM parameters including conditional binding constants and $f_{mix}^{50\%}$ are presented in Table 4.1.

$$\mathrm{EC50}_{site} = \mathrm{IS} \times \mathrm{EM}_{site} \quad (4.9)$$

$$\mathrm{IS} = \frac{EC50_{test}}{EM_{test}} = \frac{f_{mix}^{50\%}}{1-f_{mix}^{50\%}} \quad (4.10)$$

$$EM = \frac{1+K_{XH2PO4}\{H_2PO_4{}^-\}+K_{XHPO4}\{HPO_4{}^{2-}\}}{\frac{K_{XH2AsO4}}{K_{As}}\{H^+\}+K_{XHAsO4}} \quad (4.11)$$

Site-specific EC50 of *H. vulgare* was calculated by multiplying the inherent (intrinsic) sensitivity (IS) of a tested species and environmental modulator (EM) [15]. The IS was derived from the measured EC50 and chemical analysis data of the media (i.e., phosphate activities and pH) in toxicity tests. Hence, for determining the IS value (corresponding $f^{50\%}_{mix}$ value), a single EC50 of *H. vulgare* for iAs(V) obtained from toxicity test was required.

4.3. Results and discussion

4.3.1. Effect of increasing Ca^{2+} concentrations on iAs(V) toxicity to *H. vulgare*

Changes in the $EC_{50}\{HAsO_4^{2-}\}$ values with varying Ca^{2+} concentrations are shown in Figure 4.1. The $EC_{50}\{HAsO_4^{2-}\}$ of *H. vulgare* significantly decreased from 45.1 ± 4.34 to 15.0 ± 2.60 μM as the Ca^{2+} concentrations increased from 0.2 to 20 mM (Figure 4.1a). Conversely, the $EC_{50}\{HAsO_4^{2-}\}$ of *A. fischeri*, which was the species used when developing the original BLM for iAs(V), was not significantly altered although the Ca^{2+} concentrations increased from 0 to 25 mM (Figure 4.1b) [10]. This can be ascribed to the fact that the cell PM surface electrical potential (Ψ_0) of *H. vulgare* sharply increased from -53.8 to -3.3 mV.

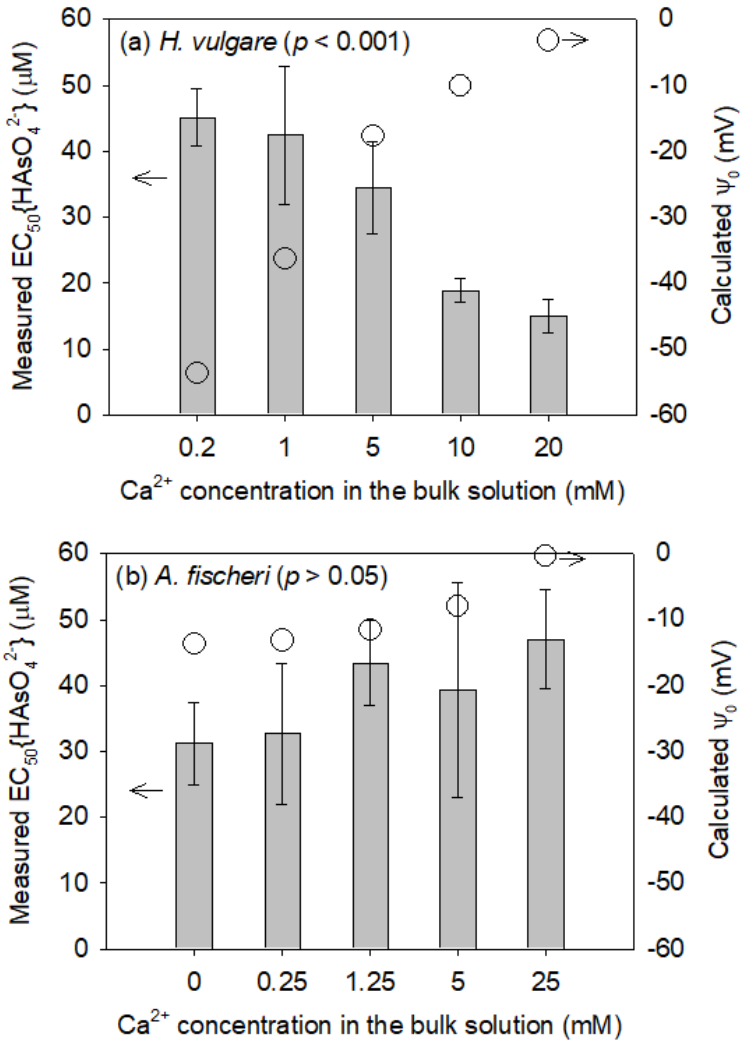

Figure 4.1. Measured EC50 values expressed as $HAsO_4^{2-}$ activity (left y-axis) obtained from (a) the root elongation test using *Hordeum vulgare*, and (b) the bioluminescence inhibition test using *Aliivibrio fischeri* (data obtained from An et al. [10]). Calculated cell membrane surface electrical potential (Ψ_0) (right y-axis) for (a) *H. vulgare*, and (b) *A. fischeri* with varying Ca^{2+} concentrations. Solid bars and error bars indicate the EC50 values, and their standard deviations (n = 3), respectively. Open circles represent the calculated Ψ_0 values. The fact that *p* value of the ANOVA test is larger than 0.05 indicates that the addition of Ca^{2+} did not significantly affect to iAs(V) toxicity.

However, only a relatively slight increase of Ψ_0 from -13.7 to -0.4 mV for *A. fischeri* was observed because the experimental solution containing 0.342 M NaCl was entirely used for the osmotic pressure control in the toxicity test using *A. fischeri*, and the solution already had a considerable amount of positive ions.

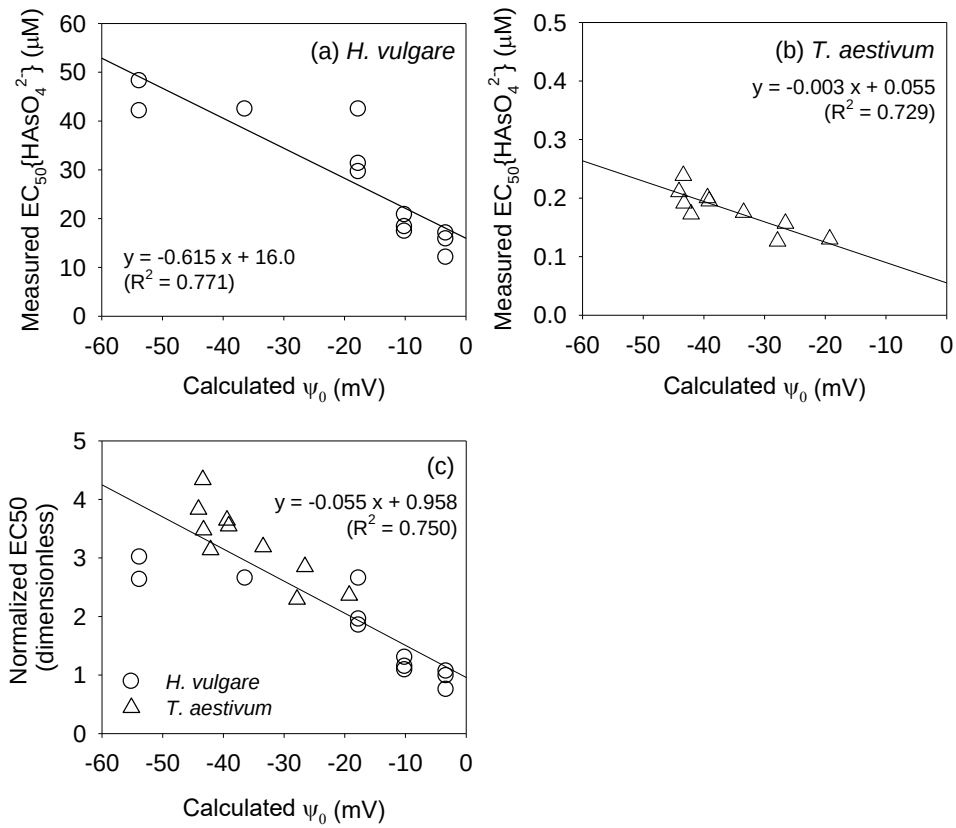

Figure 4.2. Measured EC50 values expressed as $HAsO_4^{2-}$ activity from (a) the root elongation test using *H. vulgare* conducted in this study, and (b) the root elongation test using *T. aestivum* obtained from Wang et al. [18] plotted against calculated PM surface electrical potential (Ψ_0). Normalized EC50 calculated by dividing the measured $EC_{50}\{HAsO_4^{2-}\}$ into the y-axis intercept (i.e., a situation where $\Psi_0 = 0$) of the negative linear relationship of each species presented in Figure 4.2a or 4.2b was also plotted against Ψ_0 (c) to quantify the effect of Ψ_0 by eliminating species sensitivity. The solid line represents the linear regression curve.

As reported in previous studies [17-19], an increase in Ψ_0 can accumulate more $H_2AsO_4^-$ and $HAsO_4^{2-}$ on the PM surface compared to when Ψ_0 is 0, and thus may increase iAs(V) toxicity. The $EC_{50}\{HAsO_4^{2-}\}$ of *H. vulgare* decreased 3.02 times based on the chemical properties of tested media, thus the influence of Ψ_0, which cannot be reflected by the current BLM for iAs(V), should be considered for more accurate prediction and evaluation of iAs(V) toxicity.

A negative linear relationship (slope = -0.615, R^2 = 0.771) between the calculated Ψ_0 and measured $EC_{50}\{HAsO_4^{2-}\}$ of *H. vulgare* was shown (Figure 4.2a). A similar trend was observed in wheat *T. aestivum* (slope = -0.003, R^2 = 0.729) in a study by Wang et al. [18] (Figure 4.2b). Because the slopes of the linear relationships between the calculated Ψ_0 and measured $EC_{50}\{HAsO_4^{2-}\}$ were different owing to the differences in species sensitivity to iAs(V), the normalized EC50, defined as the measured $EC_{50}\{HAsO_4^{2-}\}$ divided by the y-axis intercept of the negative linear relationship (i.e., a situation where Ψ_0 = 0), was used to quantify the effect of Ψ_0 when compensating for species sensitivity (Figure 4.2c). In this case, the same negative linear relationship (slope = -0.055, R^2 = 0.742) in both species (*H. vulgare* and *T. aestivum*) was derived. This indicates that the influence of Ψ_0 is not a plant specific property, but rather is a physicochemical property based on the attraction or repulsion of iAs(V) around the PM surface. Consequently, it was expected that the effect of Ψ_0 can be considered in a similar way for various plants, which have a negatively charged PM surface.

4.3.2. Interspecies extrapolation of BLM to predict iAs(V) toxicity to *H. vulgare*

To extrapolate the BLM, originally developed from *A. fischeri*, to barley *H. vulgare*, the IS ($f_{mix}^{50\%}$) had to first be determined. The EC50 value (i.e., $EC_{50}\{HAsO_4^{2-}\}$) of *H. vulgare* was 45.1 ± 4.34 μM, when concentrations of major cations and anions were set to background levels by adjusting the pH to 7.

Table 4.1. Conditional binding constants of the biotic ligand model (BLM) for inorganic arsenate (iAs(V)) obtained from *Aliivibrio fischeri* [10] and the calculated inherent sensitivity ($f_{mix}^{50\%}$) of terrestrial plants including barley *Hordeum vulgare*

Conditional binding constant[a]	Value (L/mol)	Species	Toxic endpoint	f_{50} (dimensionless)
log $K_{XH2AsO4}$	3.067	*Aliivibrio fischeri*	5 min bioluminescence inhibition	0.616[b]
log K_{XHAsO4}	4.802	*Hordeum vulgare*	5 d relative root elongation	0.626[c,d]
log K_{XH2PO4}	3.424	*Triticum aestivum*	2 d relative root elongation	0.015[c,e]
log K_{XHPO4}	4.588	*Cucumis sativa*	4 weeks dry weight change	0.176[c,f]
		Lactuca sativa	3 d germination rate	0.562[c,g]
		Raphanus sativa		0.649[c,g]
		Cardamine yezoensis		0.868[c,g]

[a]Conditional binding constants for iAs(V) ($HAsO_4^{2-}$ and $H_2AsO_4^-$) or phosphate (HPO_4^{2-} and $H_2PO_4^-$) bound to active binding sites on the cell membrane surface of *A. fischeri*.

[b]Obtained from An et al. [10]; [c]Calculated in this study; [d]Toxicity data obtained from this study; [e]Toxicity data obtained from Wang et al. [18]; [f]Toxicity data obtained from Lamb et al. [4]; [g]Toxicity data obtained from Ko et al. [26].

Using the calculated EM value (2.70E-05 M) in Eq. 4.11, the IS and $f_{mix}^{50\%}$ were determined as 1.675, and 0.626, respectively (Table 4.1). The calculated IS of *H. vulgare* was very similar to that of *A. fischeri* ($f_{mix}^{50\%}$ = 0.616). The IS of wheat *T. aestivum* was also calculated to assess whether it is applicable to another terrestrial plant. Wang et al. [18] reported the EC50 values of *T. aestivum* (toxic endpoint = root elongation change for 48 h) in hydroponic cultures. The calculated IS ($f_{mix}^{50\%}$) of *T. aestivum* was 0.015, which implies that the sensitivity to iAs(V) is much higher in *T. aestivum* than that in *H. vulgare*.

The extrapolated BLM to predict iAs(V) toxicity to *H. vulgare* and *T. aestivum* was validated by comparing the measured EC50 values with the predicted EC50 values (Figure 4.3). To reflect the effect of Ψ_0 described in section 4.3.1, the slopes of the negative linear relationships (p) in Figure 4.2a and Figure 4.2b were used following Eq. 4.12, when the prediction of EC50 was conducted.

$$EC_{50}\{\mathrm{HAsO_4}^{2-}\}_{site} = EC_{50}\{\mathrm{HAsO_4}^{2-}\}_{ini} + p(\Psi_{0,site} - \Psi_{0,ini}) \quad (4.12)$$

Where $EC_{50}\{HAsO_4^{2-}\}_{site}$ is the value reflecting the effect of Ψ_0 in a site, $EC_{50}\{HAsO_4^{2-}\}_{ini}$ is the predicted EC50 value from the extrapolated BLM, $\Psi_{0,site}$ is the PM surface electrical potential calculated from the water chemistry at a site, and $\Psi_{0,ini}$ is the PM surface electrical potential calculated from the water chemistry in the toxicity test solution when determining the EC50 value.

Model predicted $EC_{50}\{HAsO_4^{2-}\}$ and experimentally determined $EC_{50}\{HAsO_4^{2-}\}$

had a strong linear relationship within an order of magnitude (Figure 4.3). This demonstrated that even though only IS is considered, the site-specific iAs(V) toxicity to terrestrial plants can be predicted using water or porewater chemistry within a significant accuracy.

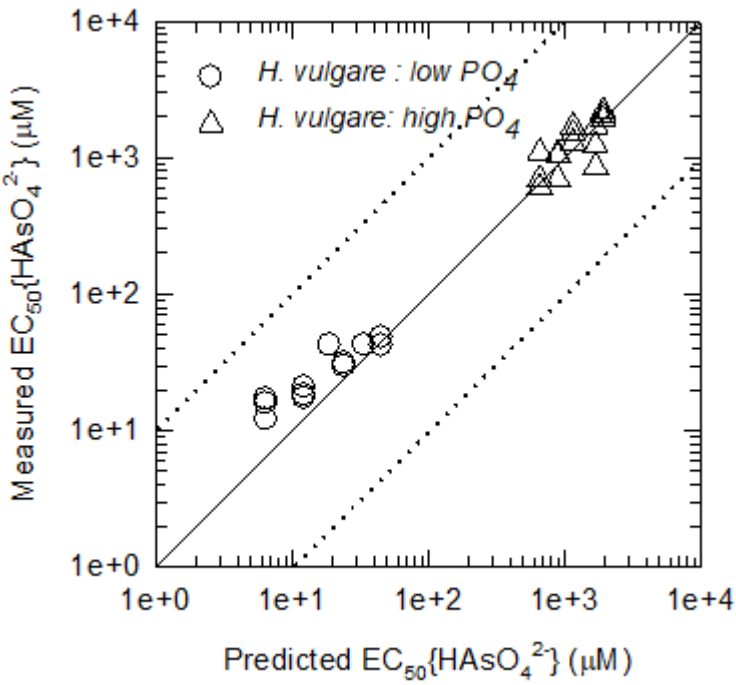

Figure 4.3. Comparison between measured $EC_{50}\{HAsO_4^{2-}\}$ and predicted $EC_{50}\{HAsO_4^{2-}\}$ by the extrapolated BLM with consideration of Ψ_0. Open circles and triangles indicate the $EC_{50}\{HAsO_4^{2-}\}$ values for the low phosphate treatment (0.05 mM) and the high phosphate treatment (5 mM), respectively. The solid line represents a perfect match between the measured and predicted EC50 values. The dashed lines indicate the difference between the measured and predicted values within an order of magnitude.

Thus, the BLM parameters for each plant species are not required i.e., the conditional binding constants between iAs(V) or phosphate and active binding sites of cell membrane are the same for both species; however, only one EC50 had to be used for sensitivity correction. To achieve better prediction accuracy, the relationship between EC50 values and Ψ_0 must be derived.

It is recognized that iAs(V) is taken up adventitiously into cells by the existing orthophosphate transporters in both prokaryotes and eukaryotes [24, 25], because iAs(V) is a chemical analog to orthophosphate. This fact speculates that there are no severe problems when the BLM parameters (e.g., conditional binding constants: $K_{XH2AsO4}$, K_{XHAsO4}, K_{XH2PO4}, and K_{XHPO4}) derived from *A. fischeri* were directly used to predict iAs(V) toxicity to terrestrial plants. The BLM for iAs(V), originally developed for *A. fischeri*, can be extrapolated to terrestrial plants including *H. vulgare* and *T. aestivum* across kingdoms.

4.4. Summary

In this study, the toxicity caused by inorganic arsenate (iAs(V)) in barley *Hordeum vulgare* was predicted using the existing biotic ligand model (BLM) for bioluminescence *Aliivibrio fischeri* via interspecies extrapolation. The extrapolated BLM, which only considered inherent sensitivity, explained the alteration of iAs(V) toxicity by the competition effect of phosphate. The 50% effective iAs(V) activity ($EC_{50}\{HAsO_4^{2-}\}$) decreased from 45.1 ± 4.34 to 15.0 ± 2.60 μM as Ca^{2+} concentration increased from 0.2 to 20 mM, owing to the accumulation of $H_2AsO_4^-$ and $HAsO_4^{2-}$ on the PM surface, which was successfully considered in the extrapolated BLM using a linear relationship between cell membrane surface electrical potential and $EC_{50}\{HAsO_4^{2-}\}$.

References

[1] B.K. Mandal, K.T. Suzuki, Arsenic round the world: a review, Talanta 58 (2002) 201-235.

[2] P.L. Smedley, D.G. Kinniburgh, A review of the source, behaviour and distribution of arsenic in natural waters, Appl. Geochem. 17 (2002) 517-568.

[3] D. Das, G. Samanta, B.K. Mandal, T.R. Chowdhury, C.R. Chanda, P.P. Chowdhury, G.K. Basu, D. Chakraborti, Arsenic in groundwater in six districts of West Bengal, India, Environ. Geochem. Health 18 (1996) 5-15.

[4] D.T. Lamb, M. Kader, L. Wang, G. Choppala, M.M. Rahman, M. Megharaj, R. Naidu, Pore-water carbonate and phosphate as predictors of arsenate toxicity in soil, Environ. Sci. Technol. 50 (2016) 13062-13069.

[5] D.A. Rubinos, V. Calvo, L. Iglesias, M.T. Barral, Acute toxicity of arsenic to *Aliivibrio fischeri* (Microtox® bioassay) as influenced by potential competitive-protective agents, Environ. Sci. Pollut. Res. 21 (2014) 8631-8644.

[6] S.D. Dyer, D.J. Versteeg, S.E. Belanger, J.G. Chaney, S. Raimondo, M.G. Barron, Comparison of species sensitivity distributions derived from interspecies correlation models to distributions used to derive water quality criteria, Environ. Sci. Technol. 42 (2008) 3076-3083.

[7] K. Lock, H. Van Eeckhout, K.A.C. De Schamphelaere, P. Criel, C.R. Janssen, Development of a biotic ligand model (BLM) predicting nickel toxicity to barley (*Hordeum vulgare*), Chemosphere 66 (2007) 1346-1352.

[8] K.A.C. De Schamphelaere, C.R. Janssen, A biotic ligand model predicting acute copper toxicity for *Daphnia magna*: The effects of calcium, magnesium, sodium, potassium, and pH, Environ. Sci. Technol. 36 (2002) 48-54.

[9] X. Wang, B. Li, Y. Ma, L. Hua, Development of a biotic ligand model for acute zinc toxicity to barley root elongation, Ecotoxicol. Environ. Saf. 73 (2010) 1272-1278.

[10] J. An, K. Nam, Extension of biotic ligand model to account for the effects of pH and phosphate in accurate prediction of arsenate toxicity, the chapter 3 of this thesis, Unpublished data (Under review in J. Hazard. Mat.).

[11] M.C. Newman, D.R. Ownby, L.C.A. Mezin, D.C. Powell, T.R.L. Christensen, S.B. Lerberg, B.-A. Anderson, Applying species-sensitivity distributions in ecological risk assessment: Assumptions of distribution type and sufficient numbers of species, Environ. Toxicol. Chem. 19 (2000) 508-515.

[12] K.A.C. De Schamphelaere, C.R. Janssen, Cross-phylum extrapolation of the *Daphnia magna* chronic biotic ligand model for zinc to the snail *Lymnaea stagnalis* and the rotifer *Brachionus calyciflorus*, Sci. Total. Environ. 408 (2010) 5414-5422.

[13] C.E. Schlekat, E. Van Genderen, K.A.C. De Schamphelaere, P.M.C. Antunes, E.C. Rogevich, W.A. Stubblefield, Cross-species extrapolation of chronic nickel biotic ligand models, Sci. Total. Environ. 408 (2010) 6148-6157.

[14] K.A.C. De Schamphelaere, D.G. Heijerick, C.R. Janssen, Cross-phylum

comparison of a chronic biotic ligand model to predict chronic toxicity of copper to a freshwater rotifer, *Brachionus calyciflorus* (Pallas), Ecotoxicol. Environ. Saf. 63 (2006) 189-195.

[15] A.J. Verschoor, J.P.M. Vink, G.R. de Snoo, M.G. Vijver, Spatial and temporal variation of watertype-specific no-effect concentrations and risks of Cu, Ni, and Zn, Environ. Sci. Technol. 45 (2011) 6049-6056.

[16] P.A. Van Sprang, F.A.M. Verdonck, F. Van Assche, L. Regoli, K.A.C. De Schamphelaere, Environmental risk assessment of zinc in European freshwaters: a critical appraisal, Sci. Total. Environ. 407 (2009) 5373-5391.

[17] P.M. Kopittke, T.B. Kinraide, P. Wang, F.P.C. Blamey, S.M. Reichman, N.W. Menzies, Alleviation of Cu and Pb rhizotoxicities in cowpea (*Vigna unguiculata*) as related to ion activities at root-cell plasma membrane surface, Environ. Sci. Technol. 45 (2011) 4966-4973.

[18] P. Wang, D. Zhou, T.B. Kinraide, X. Luo, L. Li, D. Li, H. Zhang, Cell membrane surface potential (Ψ_0) plays a dominant role in the phytotoxicity of copper and arsenate, Plant Physiol. 148 (2008) 2134-2143.

[19] Y.-M. Wang, T.B. Kinraide, P. Wang, X.-Z. Hao, D.-M. Zhou, Surface electrical potentials of root cell plasma membranes: Implications for ion interactions, rhizotoxicity, and uptake, Int. J. Mol. Sci. 15 (2014) 22661-22677.

[20] ISO. International Organization for Standardization, 1993. Soil quality—determination of the effects of pollutants on soil flora. Part 1. Method for the measurement of inhibition of root growth. No. 11269-1. ISO, Geneve.

[21] T.T.Y. Le, W.J.G.M. Peijenburg, A.J. Hendriks, M.G. Vijver, Predicting

effects of cations on copper toxicity to lettuce (*Lactuca sativa*) by the biotic ligand model, Environ. Toxicol. Chem. 31 (2012) 355-359.

[22] Gustafsson, J.P., 2014, Visual MINTEQ, Ver 3.1, available from http://vminteq.lwr.kth.se/ (accessed December, 2016).

[23] P.M. Kopittke, P. Wang, N.W. Menzies, R. Naidu, T.B. Kinraide, A web-accessible computer program for calculating electrical potentials and ion activities at cell-membrane surfaces, Plant Soil 375 (2014) 35-46.

[24] B.P. Rosen, Transport pathways for arsenic and selenium: A minireview, Environ. Int. 35 (2009) 512-515.

[25] E.M. Muehe, J.F. Eisele, B. Daus, A. Kappler, K. Harter, C. Chaban, Are rice (Oryza sativa L.) phosphate transporters regulated similarly by phosphate and arsenate?, Plant Mol. Biol. 85 (2014) 301-316.

[26] K.-S. Ko, J. Han, I.C. Kong, Assessment of arsenite, arsenate, and chromate phytotoxicity based on the activity of seed germination and growth (root & shoot) of various plant seeds, Hum. Ecol. Risk Assess. 19 (2013) 742-753.

CHAPTER 5

A Direct Measurement of Bioavailable Arsenic Concentrations Using Diffusive Gradients in Thin Film and X-ray Fluorescence Spectrometry

5.1. Introduction

Arsenic (As) contamination in soil through both natural and anthropogenic sources, including arsenic bearing minerals and wood preservatives (e.g., chromate copper arsenate), has gained the attention of scientists and regulators owing to its potential risk to human health and surrounding ecosystems [1-5]. Because soil physicochemical properties, as well as contamination history, greatly affect the bioavailability of As in soil, total As concentrations in soil do not usually reflect the bioavailability, and hence toxicity, to living organisms [6-9]. As such, it is crucial to determine bioavailable As concentrations in soil by means of an appropriate manner towards realistic risk characterization.

Significant portions of this chapter were published in An et al. ("Journal of Hazardous Materials, 260, Jinsung An, Ki-Hyun Kim, Joo-Ae Kim, Hyeyeon Jung, Hye-On Yoon, Jungju Seo, A simplified analysis of dimethylarsinic acid by wavelength dispersive X-ray fluorescence spectrometry combined with a strong cation exchange disk, 24-31, Copyright Elsevier (2013)") with permission from Elsevier.

A diffusive gradient in thin film (DGT) has been recognized as a prominent tool for assessing mobility and bioavailability of metals and metalloids in aquatic and terrestrial systems [10-15]. The principle of this technique is based on the diffusion of dissolved species through a porous material (e.g., a polyacrylamide hydrogel) and their retention on a binding resin (e.g., Chelex-100 resin). Using the DGT provides the advantages of preconcentration, time-integration, matrix interference removal, and *in situ* analysis [10,11]. The labile (bioavailable) concentration of the analyte (C_{DGT}) can be calculated from the mass accumulated in the DGT resin (M), following Eq. 5.1, on the basis of Fick's first law [15].

$$C_{DGT} = \frac{M\Delta g}{DtA} \quad (5.1)$$

Where Δg is the thickness of the gel layer (diffusion layer + filter membrane) that is determined according to the manufacturing process, D is the temperature-corrected diffusion coefficient for the analyte in a polyacrylamide hydrogel that has been normally reported by previous studies, t is the deployment time, and A is the surface area of the gel layer.

In general, the mass of analyte in the DGT resin (M) is the only unknown variable. It is eluted from the ligand using acid extraction (normally 6 N HNO_3) for 12 to 24 h, and the mass is then determined using inductively coupled plasma atomic emission

spectrometry (ICP-AES) or ICP mass spectrometry (ICP-MS). However, as the elution efficiency of the target analyte from the DGT resin is much less than 100%, predictions of its bioavailable concentration may be biased. Clearly, a direct analysis of the analyte in the DGT resin, which does not require a burdensome extraction stage, would be the preferable choice, if available.

In this respect, X-ray fluorescence spectrometry (XRF) is a potent tool due to its applicability to the analysis of most elements in various solid phase samples, with a short analyzing time and a non-destructive sample preparation procedure. Particularly, the matrix effect, including secondary excitation and absorption of the emitted X-ray, can be minimized when the analyte (on a thin layer) is analyzed using XRF. Recently, preconcentration with an appropriate thin layer-type sorbent, prior to the XRF analysis, has been widely applied to determine various elemental abundances [16-21].

Herein, we described a simple methodology to determine bioavailable As concentrations in soil by means of the combined use of DGT and XRF. In this study, the As accumulated on the DGT resin was directly analyzed using the XRF to avoid time-consuming and error-prone elution steps. Lead (Pb) was considered a major interfering element because the energy for the Kα spectrum emitted from As (10.542 keV) is comparable to that for the Lα spectrum of Pb (10.550 keV) [16], and the correction factor was derived to compensate the potential spectrum interference as presented elsewhere [16,22,23].

5.2. Materials and methods

5.2.1. Diffusive gradient in thin film (DGT)

The DGT device for soil deployment, purchased from DGT research Ltd. (Lancaster, UK), consists of a binding resin (Chelex and TiO_2 adsorbent), diffusion layer (a polyacrylamide hydrogel, thickness = 0.78 mm), and a filter membrane (pore size = 0.45 μm), tightly packed into a plastic support with an exposure window (A = 2.54 cm^2). The bioavailable As concentration in a bulk solution can be calculated by measuring the metal flux through the gel according to Eq. 5.2 [15]. Because the flux is defined as mass (M) per unit area (A) per unit time (t), Eq. 5.2 can be rewritten as Eq. 5.1.

$$F = \frac{DC_{DGT}}{\Delta g} \tag{5.2}$$

Where F is the flux of bioavailable As ions diffusing from the bulk solution to the resin (unit: $g/cm^2/s$).

The bioavailable As concentration (C_{DGT}) may be less than or equal to the total dissolved As concentration in the bulk solution, because organic and inorganic complexes of As, which have a minimal diffusion rate, can be formed [12].

5.2.2. X-ray fluorescence spectrometry (XRF)

The wavelength dispersive XRF (WDXRF) (PW2404, Phillips, Netherlands) was used to determine concentrations of As and Pb adsorbed on the DGT resin. A rhodium target X-ray tube with a 75 μm thick beryllium-window was used. The X-ray pathway was placed in a vacuum chamber (< 3 Pa) to minimize the effect of air (i.e., absorption). The diameters of X-ray collimator and aluminum sample holder used were both 27 mm. The *Bragg angles* (i.e., 2θ degree) of As-Kα, Pb-Lα, and Pb-Lβ1 were 48.781, 48.742, and 40.382°, respectively, when using a LiF220 crystal (thickness = 0.1424 nm). The instrumental conditions used in this study follow An et al. [16].

5.2.3. Calibration and the correction for spectral interference

Inorganic arsenate (iAs(V)) (100 mg-As/L) and Pb (100 mg-Pb/L) solutions were prepared by dissolving $Na_2HAsO_4{\cdot}7H_2O$ (Sigma-Aldrich, Spain) and $Pb(NO_3)_2$ (Wako, Japan), respectively, in deionized (DI) water obtained from a Milli-Q water purification system (Millipore, Bedford, MA, USA), with specific resistance of 18.2 MΩ, and stored in complete darkness at 4°C. To produce the calibration standards, the DGT devices were soaked in 100 mg/L of As and Pb solutions, respectively, at 20°C with varying deployment times. After the DGT device was retrieved from each solution, the binding resin, which contained the As and Pb, was rinsed three times with DI water, and then analyzed in two different ways. For the first method, the DGT resin was digested with a solution consisting of HCl and HNO_3 (3:1, v/v) using a microwave digester (MSP1000, CEM, USA), followed by the USEPA 3052 method

[24]. After digestion, the solution was diluted with DI water, and then filtered through 0.45-μm GHP filter. Concentrations of As and Pb in the digested solution were determined using ICP-AES (iCAP7000 Series, Thermo Scientific, USA) or ICP-MS (Agilent 7700x, Agilent, Japan). In the second method, the DGT resin was dried at room temperature (20°C) for 2 h in a desiccator with silica gel, coated with an X-ray film (Chemplex®, SE Waaler St. Stuart, FL, USA) to prevent deformation and fragmentation by the irradiating X-ray [21], and directly analyzed using the WDXRF.

To investigate the effect of Pb interference on the XRF measurement of As intensity, the DGT devices were soaked in mixed solutions of As (0.5, 5, and 50 mg-As/L) and Pb (0, 5 and 50 mg-Pb/L) during appropriate deployment times. The mass of As and Pb adsorbed on the DGT resin was determined using the two previously mentioned methods (i.e., the DGT-XRF and ICP-AES or MS after acid digestion) for comparison.

5.2.4. Preparation of freshly spiked and aged soils

Two uncontaminated soil samples were collected from surface soil (0 to 15 cm depth), air-dried, and sieved through a 2 mm mesh. Soil physicochemical properties including pH, organic matter content, cation exchange capacity, and texture are presented in Table 5.1. Soil samples were spiked with soluble iAs(V) to make the As concentration to 100 mg-As/kg-soil. Each soil was stored in a 1-L polyethylene beaker in which the moisture content was maintained as the field capacity, and the sample was aerated, and kept out of direct light at room temperature. In order to

correct the amount of evaporated water and to mimic field drying-wetting cycles, DI water was added every 10 d. Soil samples were taken at different times (1 and 500 d), air-dried, and used in phytotoxicity tests employing the DGT-XRF methodology.

Table 5.1. Physicochemical properties used in this study

Sample ID	pH	Cation exchange capacity (cmol/kg)	Organic matter (%)	Soil texture			
				Sand (%)	Silt (%)	Clay (%)	Classification
Soil A	6.9	4.5	6.3	89.4	4.2	6.4	Loamy sand
Soil B	6.9	16.3	4.4	62.2	26.9	10.9	Sandy loam

5.2.5. Phytotoxicity tests with barley *H. vulgare*

Phytotoxicity to barley *H. vulgare*, measured through root and shoot elongation, was investigated following Chae et al. [25]. After sterilization with 5% NaOCl for 10 min, each seed was rinsed three times with DI water, and exposed on wet cotton for 3 h. Seeds (n = 5) were placed in 50 g of each soil sample within a 100-mL polyethylene vial, while the field capacity of the soil was maintained. All vials were incubated at 20°C in a 16:8 light:dark photoperiod using a growth chamber (E15, Conviron, Canada) for 5 d. After the removal of the soil, the root and shoot elongation was carefully measured.

5.2.6. Application of the DGT-XRF technique to determine bioavailable As concentrations in soil

Soil samples were wetted to field capacity for 72 h before DGT deployment [15]. A soil slurry was prepared by mixing and continuously adding DI water until the maximum water retention was reached [15]. The DGT device was gently pushed onto the soil surface to achieve complete contact between the membrane of the DGT and soil particles. During the deployment, the temperature was maintained at 20°C in a growth chamber. The DGT device was retrieved from the soil after 1 h, and the binding gel removed. Then, the mass of As was determined using the XRF. The bioavailable As concentration in soil (C_{DGT}) was calculated using Eq. 5.1 with Δg = 0.78 mm, D = 4.79 × 10^{-6} cm^2/s at 20°C, A = 2.54 cm^2, t = 3600 s, and the mass of As (M, unit: μg) directly measured using the XRF.

5.3. Results and discussion

5.3.1. Calibration and analytical performance

The X-ray intensity, measured at a *Bragg angle* of 48.781°, was plotted against the As content in the DGT resin in order to draw the calibration curve for As, which showed a strong linearity (R^2 = 0.997) (Figure 5.1a). The limit of detection (LOD), defined as three times the standard deviation of the blank sample (σ, n = 7) divided by the slope of calibration curve (p) [22], was evaluated to assess the detection capacity of the DGT-XRF methodology. The LOD value was found to be 0.06 μg for

the DGT resin. The limit of quantification (LOQ, 10σ/p) was 0.20 μg, implying that it is recommended to control the DGT deployment time (t in Eq. 5.1) so that the As content adsorbed on the DGT resin is greater than 0.20 μg.

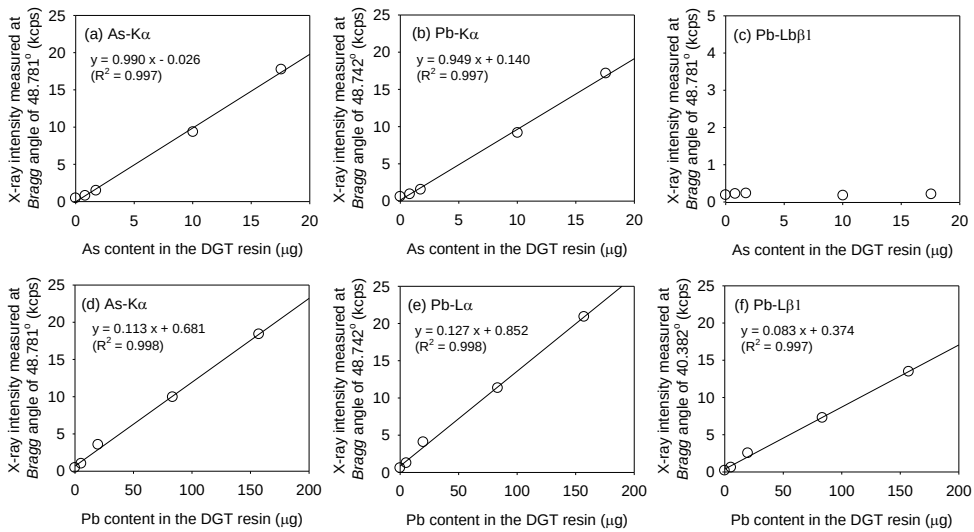

Figure 5.1. Measured X-ray intensities at the *Bragg angle* of (a) 48.781° for As-Kα, (b) 48.742° for Pb-Lα, and (c) 40.382° for Pb-Lβ1 with increasing As content (0, 0.8, 1.7, 10.0, 17.6 μg) and (d) 48.781° for As-Kα, (e) 48.742° for Pb-Lα, and (f) 40.382° for Pb-Lβ1 with increasing Pb content (0, 5.4, 19.8, 83.5, and 157 μg) in the DGT resins, when using a LiF220 crystal (2d = 0.2848 nm). Calibration of Pb was achieved by using the Pb-Lβ1 line, because overlap between Pb-Lα and As-Kα can occur due to their proximity. Solid lines indicate the linear regression curves.

5.3.2. Correction factor for compensating spectral interference of Pb

The spectral interference between As-Kα and Pb-Lα as presented in Figure 5.1b and Figure 5.1d, owing to proximity of their emission energies (i.e., 10.542 keV for As-Kα and 10.550 keV for Pb-Lα) [16], should be corrected for using a correction factor (CF) [16,22,23]. The use of a proper CF is reasonable, as the coexistence of

As and Pb has been reported for several environmental matrices [26,27]. To derive the CF value, the X-ray intensity, measured at a *Bragg angle* of 48.781° (As-Kα line) was plotted against the Pb content in the DGT resin (Figure 5.1d). Although there was no adsorption of As onto the DGT resin, the X-ray intensity significantly increased with increasing the Pb content in the DGT resin. The CF value for compensating this spectral interference was set to 0.113, which is the slope of the linear regression between the X-ray intensity, measured at a *Bragg angle* of 48.781°, and the Pb content of the DGT resin (Figure 5.1d). The initial As intensity that can be influenced by the Pb content in the DGT resin can be corrected by using Eq. 5.3.

$$I_c = I_i - (\mathrm{CF} \times [\mathrm{Pb}]_{DGT}) \quad (5.3)$$

Where I_c is the corrected As intensity (kilo count per second; kcps), I_i is the initial As intensity (kcps), and $[Pb]_{DGT}$ is the Pb content in the DGT resin (μg). The Pb content in the DGT resin can be determined using an ancillary calibration curve based on the Pb-Lβ1 line, instead of Pb-Lα (Figure 5.1f), as it cannot be influenced by the As content in the DGT resin, and so can be used to determine $[Pb]_{DGT}$ in Eq. 5.3. Although the As content in the DGT resin was altered, the X-ray intensity, measured at a *Bragg angle* of 40.382° (for Pb-Lβ1), was constant (Figure 5.1c).

Table 5.2. Comparison of the mass of As and Pb, determined by ICP-MS or ICP-AES and by the DGT-XRF methodology, with and without the CF adjustment.

Pb mass in the DGT resin (μg)		As mass in the DGT resin (μg)			X-ray intensity measured at As-Kα (kcps)	
			Using XRF			
Using ICP-OES	Using XRF	Using ICP-OES	After CF adjustment	Before CF adjustment	After CF adjustment	Before CF adjustment
< 0.12	ND[a]	0.986	1.10	1.10	1.06	1.06
5.85	5.11	0.891	1.09	1.68	1.06	1.63
11.4	9.3	6.03	6.00	7.06	5.91	6.96
15.0	16.4	0.285	0.362	2.23	0.333	2.18
42.7	45.6	9.4	10.3	15.5	10.1	15.3
43.0	39.9	1.73	1.94	6.49	1.89	6.40
181	177	< 0.24	ND	20.2	NA[b]	20.0

[a]ND = not detected; The mass of analyte adsorbed on the DGT resin was lower than the limit of detection (0.06 μg for As).

[b]NA = not applicable. The X-ray intensity was calculated as a negative number after employing the CF value.

The As and Pb contents in the DGT resin, determined using the DGT-XRF methodology, were fairly similar to those determined using ICP-OES or ICP-MS analysis after employing the CF value, as shown in Table 5.2. The relative error (RE) defined as Eq. 5.4 ranged from 0.12 to 6.8 when the CF was not applied. On the other hand, the RE ranged from 0.005 to 0.27 after CF adjustment (Table 5.2).

$$RE = \frac{|[As]_{DGT} - [As]_{ICP}|}{[As]_{ICP}} \quad (5.4)$$

Where $[As]_{DGT}$ is the As content in the DGT resin measured using the DGT-XRF methodology, and $[As]_{ICP}$ is the As content in the DGT resin measured using ICP-MS or ICP-OES after acid digestion.

5.3.3. Determination of bioavailable As concentrations in freshly spiked and aged soils

The feasibility of the proposed DGT-XRF methodology was assessed by comparing phytotoxicity tests and bioavailable As concentrations. Phytotoxicty tests with barley *H. vulgare* were conducted using two different soils spiked for 1 d (i.e., freshly spiked soil) and 500 d (i.e., aged soil) with 100 mg/kg of As. Root elongation increased from 5.67 ± 1.53 to 10.2 ± 3.97 mm for soil A, and 7.33 ± 3.79 to 32.0 ± 12.6 mm for soil B, according to incubation time (Figure 5.2a and Figure 5.2d). Also, shoot elongation increased from 0 to 5.33 ± 2.5 mm for soil A, and 0 to 11.5 ± 3.70 mm for soil B (Figure 5.2b and Figure 5.2e). Concurrently, bioavailable As concentrations in soil, determined using the DGT-XRF methodology, decreased from 23.3 ± 1.84 to 12.2 ± 1.23 μg/L for soil A, and 14.4 ± 0.939 to 10.1 ± 0.479 μg/L for soil B (Figure 5.2c and Figure 5.2f). These results indicate that, rather than total As concentrations in the soil, bioavailable As concentrations are likely to be related to the phytotoxicity of As to *H. vulgare*.

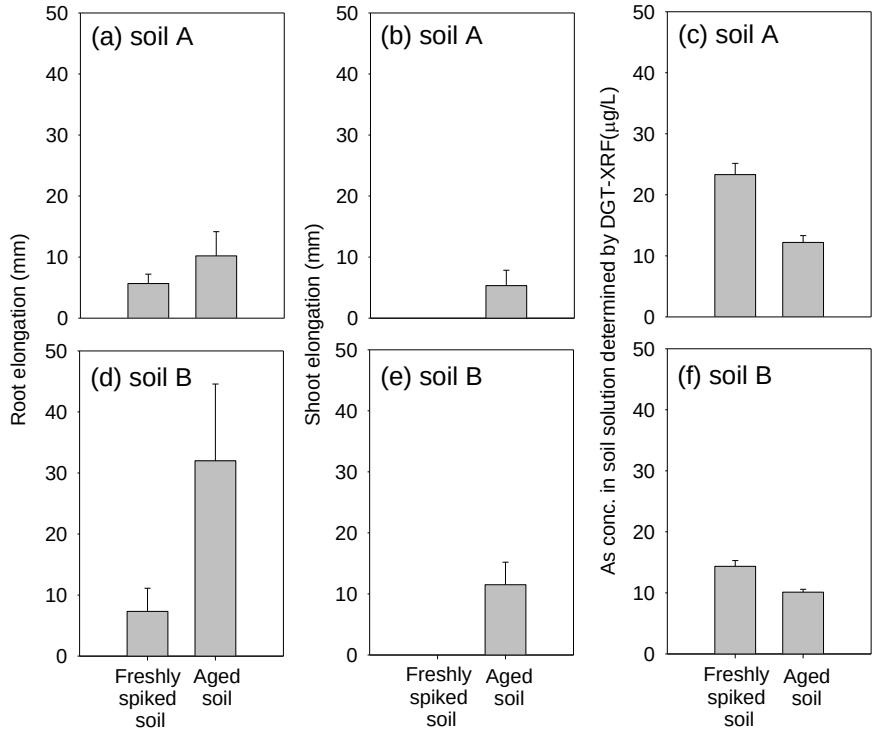

Figure 5.2. Growth of barley *Hordeum vulgare*, measured by root and shoot elongation, and bioavailable As concentrations in freshly spiked (1 d) and aged (500 d) soils determined using the DGT-XRF methodology. Error bar indicates the standard deviation (n = 3).

The aging processes are considered to be related a gradual shift from the formation of outer-sphere complexes (electrostatically driven) between metals/metalloids and soil particles, to inner-sphere complexes (chemically driven) with increasing incubation time [6, 28]. In addition, diffusion of metals/metalloids into micropores in the soil is likely to result in alleviated lability [29]. In this study, phytotoxicity to *H. vulgare* significantly decreased as reaction time increased between 1 and 500 d, although the total As concentrations remained constant. This

demonstrated that the lability and bioavailability of As in soils was alleviated via the aging phenomenon. By using the DGT-XRF methodology, the bioavailable As concentrations in both freshly spiked and aged soils can be effectively determined, whilst eliminating time-consuming and complicated sample handling procedures, as well as moving towards more environmentally friendly analytical chemistry by reducing the use of solvents [30].

5.4. Summary

A simple and rapid method based on the combination of XRF and DGT was proposed for the analysis of bioavailable As in soil. The DGT provides an extremely simple method for separating labile and bioavailable As from soils, and allows direct preparation of the specimen for XRF analysis without the need for any pretreatment steps. As a result of the *in situ* sample preparation, this method also minimizes the probability of the transformation of labile As during sample storage, prior to chemical analysis. The DGT-XRF system achieved the LOD of 0.06 μg. The CF was derived as 0.113, and can effectively balance the spectral interference of Pb. The phytotoxicity of As to barley *H. vulgare* seems to be related to bioavailable As concentrations in both freshly spiked and aged soils, which were determined by means of the combined use of DGT and XRF, rather than total As concentrations in soils. The developed methodology can eliminate the elution step, thereby minimizing the use of solvents, making this method more environmentally friendly.

References

[1] P.L. Smedley, D.G. Kinniburgh, A review of the source, behaviour and distribution of arsenic in natural waters, Appl. Geochem. 17 (2002) 517-568.

[2] V.K. Sharma, M. Sohn, Aquatic arsenic: Toxicity, speciation, transformations, and remediation, Environ. Int. 35 (2009) 743-759.

[3] J. Susaya, K.-H. Kim, M.C. Jung, The impact of mining activities in alteration of As levels in the surrounding ecosystems: An encompassing risk assessment and evaluation of remediation strategies, J. Hazard. Mater. 182 (2010) 427-438.

[4] C.C. Tanner, J.S. Clayton, Persistence of arsenic 24 years after sodium arsenite herbicide application to Lake Rotoroa, Hamilton, New Zealand, New Zeal. J. Mar. Fresh. 24 (1990) 173-178.

[5] J.A. Hingston, C.D. Collins, R.J. Murphy, J.N. Lester, Leaching of chromated copper arsenate wood preservatives: a review, Environ. Pollut. 111 (2001) 53-66.

[6] X.-Y. Tang, Y.-G. Zhu, X.-Q. Shan, R. McLaren, J. Duan, The ageing effect on the bioaccessibility and fractionation of arsenic in soils from China, Chemosphere 66 (2007) 1183-1190.

[7] S. Liang, D.-X. Guan, J. Li, C.-Y. Zhou, J. Luo, L.Q. Ma, Effect of aging on bioaccessibility of arsenic and lead in soils, Chemosphere 151 (2016) 94-100.

[8] A.L. Juhasz, E. Smith, J. Weber, R. Naidu, M. Rees, A. Rofe, T. Kuchel, L. Sansom, Effect of soil ageing on in vivo arsenic bioavailability in two dissimilar soils, Chemosphere 71 (2008) 2180-2186.

[9] J. Song, F.-J. Zhao, S.P. McGrath, Y.-M. Luo, Influence of soil properties and aging on arsenic phytotoxicity, Environ. Toxicol. Chem. 25 (2006) 1663-1670.

[10] W. Davison, H. Zhang, *In situ* speciation measurements of trace components in natural waters using thin-film gels, Nature 367 (1994) 546-548.

[11] H. Zhang, W. Davison, Performance characteristics of diffusion gradients in thin films for the *in situ* measurement of trace metals in aqueous solution, Anal. Chem. 67 (1995) 3391-3400.

[12] H. Zhang, W. Davison, Direct in situ measurements of labile inorganic and organically bound metal species in synthetic solutions and natural waters using diffusive gradients in thin films, Anal. Chem. 72 (2000) 4447-4457.

[13] B. Nowack, S. Koehler, R. Schulin, Use of diffusive gradients in thin films (DGT) in undisturbed field soils, Environ. Sci. Technol. 38 (2004) 1133-1138.

[14] S. Zhang, P.N. Williams, C.-Y. Zhou, L.Q. Ma, J. Luo, Extending the functionality of the slurry ferrihydrite-DGT method: Performance evaluation for the measurement of vanadate, arsenate, antimonite and molybdate in water, Chemosphere 184 (2017) 812-819.

[15] D. Menezes-Blackburn, H. Zhang, M. Stutter, C.D. Giles, T. Darch, T.S. George, C. Shand, D. Lumsdon, M. Blackwell, C. Wearing, P. Cooper, R.

Wendler, L. Brown, P.M. Haygarth, A holistic approach to understanding the desorption of phosphorus in soils, Environ. Sci. Technol. 50 (2016) 3371-3381.

[16] J. An, K.-H. Kim, J.-A. Kim, H. Jung, H.-O. Yoon, J. Seo, A simplified analysis of dimethylarsinic acid by wavelength dispersive X-ray fluorescence spectrometry combined with a strong cation exchange disk, J. Hazard. Mater. 260 (2013) 24-31.

[17] J. An, H. Jung, J.-R. Bae, H.-O. Yoon, J. Seo, Feasibility of wavelength dispersive X-ray fluorescence spectrometry for a simplified analysis of bromine in water samples with the aid of a strong anion exchange disk, Spectrochim. Acta B 91 (2014) 1-4.

[18] J. Lee, J. An, J.-A. Kim, H.-O. Yoon, Effectiveness of activated carbon disk for the analysis of iodine in water samples using wavelength dispersive X-ray fluorescence spectrometry, Chemosphere 142 (2016) 72-76.

[19] E. Margui, M. Hidalgo, I. Queralt, K. Van Meel, C. Fontas, Analytical capabilities of laboratory, benchtop and handheld X-ray fluorescence systems for detection of metals in aqueous samples pre-concentrated with solid-phase extraction disks, Spectrochim. Acta B 67 (2012) 17-23.

[20] T. Inui, W. Abe, M. Kitano, T. Nakamura, Determination of Cr(III) and Cr(VI) in water by wavelength-dispersive X-ray fluorescence spectrometry after preconcentration with an ion-exchange resin disk, X-Ray Spectrom. 40 (2011) 301-305.

[21] W. Abe, S. Isaka, Y. Koike, K. Nakano, K. Fujita, T. Nakamura, X-ray fluorescence analysis of trace metals in environmental water using

preconcentration with an iminodiacetate extraction disk, X-Ray Spectrom. 35 (2006) 184-189.

[22] J. An, K.-H. Kim, H.-O. Yoon, J. Seo, Application of the wavelength dispersive X-ray fluorescence technique to determine soil fluorine with consideration of iron content in the matrix, Spectrochim. Acta B 69 (2012) 38-43.

[23] J. An, J. Lee, H.-O. Yoon, Strategies for overcoming limitations associated with fluorine determination in solid materials by conventional wavelength dispersive X-ray fluorescence spectrometry, Microchem. J. 122 (2015) 76-81.

[24] USEPA (United States Environmental Protection Agency), Method 3052 - Microwave Assisted Acid Digestion of Siliceous and Organically Based Matrices, 1996.

[25] Y. Chae, D. Kim, Y.-J. An, Effects of fluorine on crops, soil exoenzyme activities, and earthworms in terrestrial ecosystems, Ecotoxicol. Environ. Saf. 151 (2018) 21-27.

[26] F.J. Peryea, T.L. Creger, Vertical distribution of lead and arsenic in soils contaminated with lead arsenate pesticide residues, Water Air Soil Pollut. 78 (1994) 297-306.

[27] P.N. Williams, M. Lei, G. Sun, Q. Huang, Y. Lu, C. Deacon, A.A. Meharg, Y.-G. Zhu, Occurrence and Partitioning of Cadmium, Arsenic and Lead in Mine Impacted Paddy Rice: Hunan, China, Environ. Sci. Technol. 43 (2009) 637-642.

[28] P.C. Zhang, D.L. Sparks, Kinetics selenite and selenite

adsorption/desorption at the goethite/water interface using pressure-jump relaxation, Environ. Sci. Technol. 24 (1990) 1848-1856.

[29] L. Axe, P. Trivedi, Intraparticle surface diffusion of metal contaminants and their attenuation in microporous amorphous Al, Fe, and Mn oxides, J. Colloid Interf. Sci. 247 (2002) 259-265.

[30] S. Armenta, S. Garrigues, M. de la Guardia, Green analytical chemistry, Trac-Trend. Anal. Chem. 27 (2008) 497-511.

CHAPTER 6

Conclusions

The effectiveness of *in situ* stabilization, as a risk mitigation measure, in the arsenic (As)-contaminated soil should be evaluated by means of both chemical extractability and biological responses, as chemical analysis alone may not be sufficient to assess the ecotoxicity. Although bioassays are liable and realistic in determining As toxicity in soil, they are time-consuming and costly. As an alternative, biotic ligand model (BLM) was developed to predict the site-specific toxicity of inorganic arsenate (iAs(V)) in soil porewater by using the bioluminescent bacteria *Aliivibrio fischeri*. To enhance the accuracy of the BLM, the effects of major cations/anions and pH were assessed, and incorporated into the BLM. Phosphates ($HPO_4^{2-}/H_2PO_4^-$) competition effect, which was commonly found in soil porewater, was incorporated into the BLM. Parameters of BLM including conditional binding constants of iAs(V) and phosphate to active binding sites on the surface of *A. fischeri*, and the fraction of active binding sites occupied by iAs(V) ions to induce 50% toxicity were determined. As a consequence, site-specific 50% effective concentrations (EC50) can be predicted by using BLM for iAs(V) with soil porewater chemistry data. This type of approach can be extended to a higher terrestrial plant (barley *Hordeum vulgare*) with the aid of interspecies extrapolation

of BLM. Through the calculation of iAs(V) activity near the root cell plasma membrane surface of *H. vulgare*, the fact that the iAs(V) toxicity increased as increasing Ca^{2+} concentrations can be successfully incorporated into the BLM for *H. vulgare*. Also, the free iAs(V) concentration in soil can be simply and rapidly analyzed by the combined use of DGT and X-ray fluorescence spectrometry. By compensating Pb interference with the aid of the correction factor derived in this study, the accurate labile iAs(V) concentrations in soil can be determined, which is highly correlated with phytotoxicity to *H. vulgare*.

In order to derive site-specific 5% hazardous concentration (HC5), the entire normalized ecotoxicity dataset are required. This approach assumes that some species may also share BLM parameters (i.e., conditional binding constants between free metal ions or major cations and active binding sites (i.e., biotic ligand; BL) at the cell membrane surface of the organism). By following procedures in Figure 6.1, the site-specific HC5 can be calculated from the developed BLM in conjunction with the chemical analysis data of the soil porewater (soil solution). It may be able to provide a rapid and cost-effectiveness ecological risk characterization means.

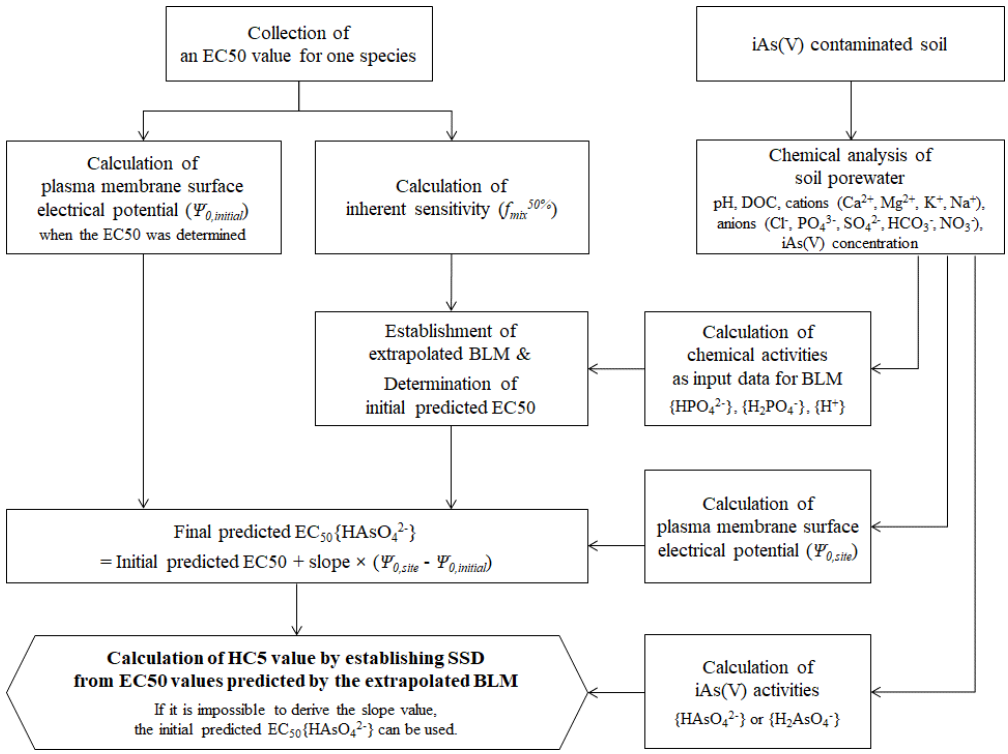

Figure 6.1. Procedures for calculating HC5 values from the physicochemical properties of iAs(V) contaminated site and the extrapolated BLM with considering the effect of PM electrical potential (Ψ_0).

국문초록

Aliivibrio fischeri 및 *Hordeum vulgare*에 대한 비소의 현장특이적 생태위해성 예측을 위한 biotic ligand model의 확장

비소오염토양의 위해도 저감방법 중 하나인 원위치 안정화(*in situ* stabilization)의 효과를 평가하기 위해서는 화학적 추출 가능성뿐만 아니라 생태독성 또한 분석되어야 한다. 생물검정법을 이용한 토양독성평가는 신뢰성이 높지만, 시간과 비용이 많이 소요된다. 따라서 본 연구에서는 기존의 biotic ligand model(BLM)을 확장하여 +5가 무기비소(iAs(V))의 현장특이적 독성을 예측하고자 하였다. BLM 파라미터를 산출하기 위해 발광성 미생물인 *Aliivibrio fischeri*를 사용하였다. 우선, 다양한 환경인자(i.e., 주요 양이온(Ca^{2+}, Mg^{2+}, K^{+}), 주요 음이온(HPO_4^{2-}/$H_2PO_4^{-}$, SO_4^{2-}, NO_3^{-}, HCO_3^{-}), pH)가 iAs(V)의 독성에 미치는 영향을 확인하였다. HPO_4^{2-}의 활성도(activity)가 0에서 0.44 mM로 증가함에 따라 $EC_{50}\{HAsO_4^{2-}\}$(50%의 발광성이 저해되는 $HAsO_4^{2-}$의 활성도)가 31 ± 6에서 859 ± 128 μM로 증가했다. 이는 PO_4와 iAs(V) 사이의 구조적 유사성이 *A. fischeri* 표면의 활성결합부위(active binding site)에 대해 경쟁효과를 발휘함을 의미한다. Ca^{2+}, Mg^{2+}, K^{+}, SO_4^{2-},

NO_3^-, 및 HCO_3^-의 활성도 증가는 iAs(V)의 독성에 통계적으로 유의한 영향을 미치지 않았다. 한편, pH가 5에서 9로 증가함에 따라 $EC_{50}[As]_T$(50%의 발광성이 저해되는 iAs(V)의 농도)가 3,554 ± 393에서 39 ± 6 μM로 감소하였고, 이는 $H_2AsO_4^-$ 보다 $HAsO_4^{2-}$가 *A. fischeri*에 더 높은 독성을 발현함을 의미한다. PO_4의 경쟁효과와 pH에 의한 비소 종 변화에 따른 iAs(V)의 독성 변화를 반영할 수 있는 BLM 기반 비소 독성예측모형의 매개변수를 결정하기 위해, pH 5와 pH 9에서 PO_4의 활성도(pH 5에서는 $H_2PO_4^-$, pH 9에서는 HPO_4^{2-}가 존재)를 달리하며 얻은 독성데이터(발광성 저해정도)를 이용하였다. 결정된 매개변수는 각각 $f_{mix}^{50\%}$ = 0.616, $\log K_{XH2PO4}$ = 3.424, $\log K_{XHPO4}$ = 4.588, $\log K_{XH2AsO4}$ = 3.067 및 $\log K_{XHAsO4}$ = 4.802 이다.

이러한 유형의 접근법은 종간외삽법(interspecies extrapolation)을 통해 보리 *Hordeum vulgare*와 같은 고등식물에도 확장/적용될 수 있다. 고유민감도(inherent sensitivity)만을 고려한 외삽된 BLM은 PO_4의 경쟁효과에 의한 iAs(V)의 독성변화를 잘 설명할 수 있었다. 또한, Ca^{2+}의 농도가 0.2에서 20 mM으로 증가함에 따라, 세포막 표면에 $H_2AsO_4^-$와 $HAsO_4^{2-}$가 축적되어 $EC_{50}\{HAsO_4^{2-}\}$ 값이 45.1 ± 4.34에서 15.0 ± 2.60 μM으로 감소한다는 사실은, 세포막 표면의 전위(electrical potential)와 $EC_{50}\{HAsO_4^{2-}\}$ 사이의 선형관계를 사용하여 외삽된 BLM에 성공적으로 반영될 수 있었다.

토양 중 생물학적이용성이 높은 비소의 농도를 측정하는 방법을 단순화하기 위해, X-선 형광분석법(X-ray fluorescence spectrometry; XRF)을 사용하여 diffusive gradients in thin film(DGT)에 이용되는 결합수지(binding resin)의 직접분석 가능성을 확인하였다. DGT로부터 분리한 결합수지는 25° C에서 2시간 동안 건조시킨 후, XRF로 직접 분석하였다. DGT의 결합수지 내 비소의 질량과 그에 따른 X-선 강도는 강한 선형성(결정 계수; R^2 = 0.997)을 나타냈고, 검출한계가 0.06 μg인 검정곡선을 생성할 수 있었다. Pb에 의한 간섭효과를 제거하기 위해, 결합수지 내 Pb의 질량에 따른 *Bragg* 각도 48.781° 에서 측정되는 X-선 강도를 비교하였고, 이를 통해 보정계수 0.113을 산출하였다. 보정계수를 이용할 경우, Pb의 간섭효과를 효과적으로 배제할 수 있었다.

본 연구에서 개발한 확장된 BLM과 토양공극수 분석결과를 이용하여 비소오염토양의 독성 또는 생물학적이용성을 효과적으로 평가할 수 있으리라 기대된다.

주요어: +5가 무기비소, biotic ligand model, diffusive gradients in thin film, 종간외삽법, 토양공극수

학번: 2014-31121